AD-A083 609 CALIFORNIA INST OF TECH PASADENA GRADUATE AERONAUTIC--ETC F/G 11/9
DYNAMIC FRACTURE IN VISCOELASTIC SOLIDS.(U)
MAR 80 M C GUPTA, W G KNAUSS N00014-78-C-0634
UNCLASSIFIED GALCIT-SM-80-5 NL

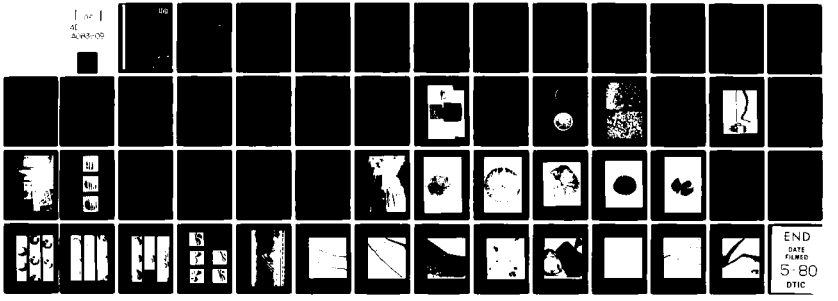

(12)

LEVEL

DYNAMIC FRACTURE IN VISCOELASTIC SOLIDS

Mool C. Gupta
Wolfgang G. Knauss

First Annual Report
August 1978 - August 1979

This work is supported by the Office of Naval Research,
Department of the Navy through Contract #N00014-78-C-0634

California Institute of Technology
Graduate Aeronautical Laboratories
Pasadena, California 91125

SECURITY CLASSIFICATION OF THIS PAGE (When Data Entered)

REPORT DOCUMENTATION PAGE

READ INSTRUCTIONS BEFORE COMPLETING FORM

1. REPORT NUMBER: First Annual Report
2. GOVT ACCESSION NO.: AD-A083609
3. RECIPIENT'S CATALOG NUMBER:

(6) 4. TITLE (and Subtitle): DYNAMIC FRACTURE IN VISCOELASTIC SOLIDS

5. TYPE OF REPORT & PERIOD COVERED: Annual Technical Report

6. PERFORMING ORG. REPORT NUMBER: SM Report 80-5

7. AUTHOR(s): M. C. Gupta, W. G. Knauss

(15) 8. CONTRACT OR GRANT NUMBER(s): N00014-78-C-0634

9. PERFORMING ORGANIZATION NAME AND ADDRESS: California Institute of Technology, Pasadena, California 91125

10. PROGRAM ELEMENT, PROJECT, TASK AREA & WORK UNIT NUMBERS:

11. CONTROLLING OFFICE NAME AND ADDRESS:

(11) 12. REPORT DATE: Mar[redacted]80

13. NUMBER OF PAGES: 48

14. MONITORING AGENCY NAME & ADDRESS (if different from Controlling Office):
(10) Mod 1 G1/Gupta
Wolfgang G1/Knauss

15. SECURITY CLASS. (of this report): Unclassified

15a. DECLASSIFICATION/DOWNGRADING SCHEDULE:

16. DISTRIBUTION STATEMENT (of this Report)

Approved for public release; distribution unlimited.

(12) 53

17. DISTRIBUTION STATEMENT (of the abstract entered in Block 20, if different from Report)

(9) Annual rept. no. 1, Aug 78 - Aug 79

18. SUPPLEMENTARY NOTES

(14) GALCIT-SM-80-5

19. KEY WORDS (Continue on reverse side if necessary and identify by block number)

Failure, Elastomer, Polyurethane, Solithane, Filled, Unfilled, Particulate Material, Viscoelastic, Shear Creep Compliance, Crack Propagation, Dynamic Loading, Wave Propagation, Strain Gauge, Photoelastic, High Speed Cinematography, Electromagnetic Loading Device, Fracture Surface.

20. ABSTRACT (Continue on reverse side if necessary and identify by block number)

The purpose of our studies is to gain fundamental information on the failure of elastomers, both unfilled and filled with particulate material; specially to determine the amount of fragmentation that occurs on failure under dynamic conditions. Experimental information sought relates to crack velocity and crack branching.

At present we are studying the onset of crack propagation, and possible crack branching in elastomers using high speed cinematography under loads

DD FORM 1 JAN 73 1473 EDITION OF 1 NOV 65 IS OBSOLETE

137700

SECURITY CLASSIFICATION OF THIS PAGE (When Data Entered)

induced with an electromagnetic loading device. In this report we describe the material preparation, experimental technique and some preliminary results obtained on crack growth in Solithane (a polyurethane elastomer).

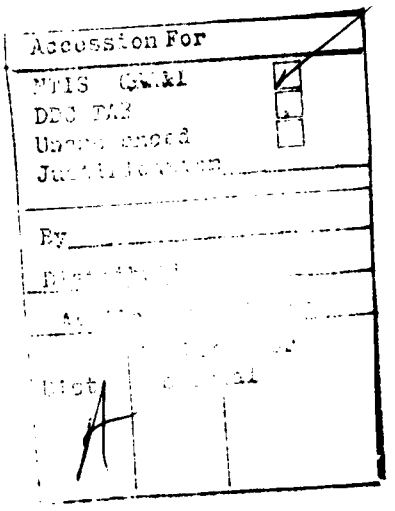

DYNAMIC FRACTURE IN VISCOELASTIC SOLIDS

Mool C. Gupta
Wolfgang G. Knauss

First Annual Report
August 1978 - August 1979

This work is supported by the Office of Naval Research,
Department of the Navy through Contract #N00014-78-C-0634

California Institute of Technology
Graduate Aeronautical Laboratories
Pasadena, California 91125

ABSTRACT

The purpose of our studies is to gain fundamental information on the failure of elastomers, both unfilled and filled with particulate material; specially to determine the amount of fragmentation that occurs on failure under dynamic conditions. Experimental information sought relates to crack velocity and crack branching.

At present we are studying the onset of crack propagation, and possible crack branching in elastomers using high speed cinematography under loads induced with an electromagnetic loading device. In this report we describe the material preparation, experimental technique and some preliminary results obtained on crack growth in Solitane (a polyurethane elastomer).

I. INTRODUCTION

Fracture of a viscoelastic material is a function of both time and state of stress (1, 2). In metals the energy dissipation mechanism is plastic deformation and hence is essentially rate independent. Fracture in viscoelastic media on the other hand is governed by viscous dissipation and hence shows a much more pronounced time dependence. Our interest here is in determining the fracture behavior of viscoelastic material at high rates of loading. Material at high strain rates is governed by molecular relaxation process. With a rising deformation speed the material stiffness increases and the strength of viscoelastic material changes. The increase of strain rate is equivalent to a lowering of the temperature. However, with regard to the fracture process we do not know the relation between the rate of loading on the boundary and an equivalently lower temperature.

From our shear creep compliance measurements made on Solithane, we find that the shear modulus is on the order of 10^4 psi for deformation speeds of 10^5% per second, as compared to about 500 psi at, say, 1% per second. At such high strain rates the viscoelastic behavior will therefore strongly influence the fracture behavior of Solithane. We are now trying to determine experimentally the crack growth behavior in Solithane under such high strain rates.

II. MATERIAL PREPARATION

In order to examine the effect of viscoelasticity on crack propagation it is necessary to use experimental material which exhibit distinctly viscoelastic behavior under high rates of strain. One material which has been chosen is Solithane 113 (3). Solithane 113 is the trade name for a polyurethane elastomer manufactured by the Thiokol Chemical Corporation. It is furnished in two components, a so-called urethane resin and catalyst. By mixing the two components in various ratios the mechanical properties of the final elastomer can be varied over a considerable range.

After an extensive amount of cleaning and redesigning the Solithane casting facility is in operation. Figure 1 shows a photograph of the casting facility. We have made several improvements on the casting facility from the previous design. Now the catalyst and resin are mixed in proportion by weight rather than by volume. We have also improved the method of mixing of catalyst and resin. We have cast about eight plates of Solithane of size 12 x 12 x 0.25 in. (fig. 2). These plates are free of air bubbles and are generally of good optical quality. We have also cast some specimens for Dr. Y. M. Gupta at the Stanford Research Institute. Solithane specimens have been cast and sent to Dr. Schnur (NRL) and to Dr. Pae (Rutger's University).

We have experimented with glass bead filled Solithane to simulate solid propellant material. Glass beads of size 50-100 μm were obtained from the Cataphoto Division of the Ferro Corporation. Solithane specimens with various proportions of glass beads in it were prepared. A typical glass bead filled Solithane specimen is shown in fig. 3. It is obvious from fig. 3 that glass bead filled Solithane specimens are not transparent. Figure 4 shows the photograph of glass beads; it is clear that all beads are not

spherical and there appears to be air pockets trapped in some glass beads. When a high proportion of glass beads (higher than 50% by weight of total) are used, mixing and making air bubble-free specimens becomes a problem. Solithane specimens containing in proportion 50% by weight of glass beads have been prepared. Glass beads have a tendency to settle down during the curing process which creates a nonuniform distribution of glass beads in the Solithane specimen. By rotating the Solithane during the curing process in the oven, we were able to make Solithane specimens with a uniform distribution of glass beads. Glass beads have been supplied to Dr. P. Dreyfuss for her work at the University of Akron.

III. MATERIAL CHARACTERIZATION

In order to understand the fracture behavior of Solithane, it is necessary to mechanically characterize this material. Some of the measurements which we have made on this material are discussed below.

(a) Wave propagation measurement

In contrast to elastic solids, waves in viscoelastic solids are highly attenuated. The attenuation depends strongly on the frequency and on how close the material is to the glass transition temperature. We know that stress wave propagation is a prime phenomenon associated with dynamic fracture so we have attempted to obtain an estimate of this in the time range of our experiment.

(i) Strain gage method.

For exploration work we used strain gages to pick up the passage of wave signals. The experimental arrangement for these measures is shown in fig. 5. The projectile provides a trigger signal for the oscilloscope and also the impact pulse by interrupting the laser beam. The passage of a stress wave signal picked up by each strain gage after amplification is given to a dual trace storage oscilloscope. The signals obtained from each strain gage is shown in fig. 6. The top trace is a recording of the strain gage closest to the particle impact point while the lower trace corresponds to that obtained from the second stage. Note that the initial positions of the traces are similar but that some lengthening of the time scale in the signals has occurred which is indicative of material dispersion. In this way we find that a signal induced by a pulse of duration of a few milliseconds travels with a speed of 7000 in/sec. We have also tried to measure the wave propagation with our electromagnetic loading device in conjunction with strain

gages. However, we found that the specimen size did not allow placement of the foil gages to avoid electromagnetic disturbances resulting from the pulse excitation.

(ii) Photoelastic method

Photoelastic techniques are useful experimental tools for the determination of stress distributions in structures of complex geometry (4). We have determined the behavior of stress wave propagation in Solithane using photoelasticity. The experimental arrangement used for such determinations is shown in fig. 7. Laser light is circularly polarized after passing through a spatial filter by a combination of polarizer and a quarter wave plate. The circularly polarized light passes through the birefringent material (Solithane) and then through another circular polariscope (dark field arrangement). Due to the phase shift introduced by the birefringent material, dark and bright fringes are observed. The fringes are focussed on a film track by a combination of a lens system. The movement of fringes due to stress wave propagation in the material is recorded by a high speed camera. The stress pulse on the specimen was obtained using an electromagnetic loading device as shown in fig. 8. The fringes recorded in Solithane at a framing rate of 50,000 frames/sec are shown in fig. 9. From the position of fringes as a function of time, the fringe velocity was determined. A curve of displacement versus time for different fringe order is shown in fig. 10. Having demonstrated that this recording method is feasible it remains now to relate the fringes to stress values through a photoviscoelastic characterization. That work is planned for later.

(b) Shear creep compliance measurement

In order to understand the fracture behavior of Solithane under high

strain rates it is necessary to know the relaxation modulus or creep compliance of this material at appropriate strain rates. Shear creep compliance measurements were made using a torsiometer. Cylindrical sepcimens of gage length 2.0 in. were cast for shear creep measurements. Measurements were made at different temperatures (below and above the glass transition temperature of Solithane) as shown in fig. 11. Using the time-temperature superposition principle, a master curve was obtained as shown in fig. 12. At room temperature with almost zero strain rate the shear modulus is about 140 psi, while the modulus at strain rates of 10^5%/sec is about 10^4 psi. This agrees well with the calculated creep data from the relaxation data for Solithane 113 (50% resin and 50% catalyst by volume) in ref. (3). This result also falls in line with Dr. Schnur's data.

IV. CRACK PROPAGATION STUDY

An Argon ion laser with a continuous light power of 5 watt and pulsed power of 50 watt has been obtained from Spectra Physics and is now in operation. The time coordination of laser with the electromagnetic loading device and high speed camera has been affected (fig. 13). The experimental set-up for dynamic fracture study is shown in fig. 14. We have demonstrated that we can record events at 100,000 frames/sec in transmission and reflected light. We have taken a high speed photograph under transmission light of a wire grid at a framing rate of 100,000 frames/sec. (fig. 15). A wire of diameter 0.003 inches could be easily seen in a high speed photograph taken under transmission light at a framing rate of 100,000 frames/sec. Figure 16 shows the photograph of a grid taken under a reflected light at a framing rate of 100,000 frames/sec. For this test run the reflecting surface was an aluminum plate coated with white glossy paint. The exposure time (the laser light pulse width) was 15 nanoseconds with an initial light intensity of 40 watts. In reflected light the light intensity becomes a problem because there is a light loss in the beam expander with a pinhole, collecting optics and the paint reflects only less than one percent of the incident light. After tuning the pulsed laser to its maximum capability and minimizing the loses in optics a high speed photograph under reflected light could be obtained.

From our first series of dynamic crack propagation experiments, fig. 17 shows a photograph of the region just ahead of the crack tip in Solithane with a curious optical structure. This type of optical structure created a big problem for us in monitoring the crack propagation in Solithane. We found that this existed with noncoherent light and even with unpolarized light.

In order to determine whether this phenomenon is the result of a surface or bulk effect we looked at the image under reflected light and noticed small irregularities. It appeared that surface irregularities on a very fine scale caused light interference patterns.

Consequently, we removed the photographic plates usually used for casting and instead used a polished aluminum mold. We also improved our mixing of the resin/catalyst mixture; mixing was performed at higher temperature. After a series of attempts now we have made Solithane plates which are optically clear and free of these disturbances. Figure 18 shows the static photograph of a crack tip in Solithane. The dark region ahead of the crack tip is a caustic. When a polaroid analyzer is inserted in the optical path the photoelastic fringes can be seen as is shown in fig. 19 (non-symmetrical loading of crack tip).

We have experimented with 12 x 12 x 1/4 in. Solithane sheets in our electromagnetic loading device. In eight tests we were unable to propagate a crack under indicated stress levels of 4365 psi. The same geometry made of plexiglass fractured at a stress level of 3144 psi (fig. 20). It appears that the relatively soft material cannot exploit fully the electromagnetic pressure. The two legs of the conductor strip separate during the experiment and thus reduce the electromagnetic force driving these apart. We have calculated the value of electromagnetic force for different separation values of copper trip.

When two conducting strips, each of width w, are separated by a thin insulator of magnetic permeability μ, the perpendicular force per unit area σ_o, resulting from the current i flowing in opposite directions is given by

$$\sigma_o = \frac{1}{2} \mu \left(\frac{i}{w}\right)^2 \qquad (1)$$

This expression is valid if a) the current is conducted in a sheet of zero thickness and b) the width of the copper strip w is much larger than the separation distance between the strips. Because Solithane is relatively soft the copper strip separation becomes relatively large during dynamic loading, which in turn reduces the instantaneous electromagnetic force. We did not encounter such a severe problem with our previous work on Homalite.

Let us calculate the variation of electromagnetic force as a function of copper strip separation. If s is the spacing between the strips (assuming them to be thin conductors) then the perpendicular force per unit area is

$$\sigma_1 = \frac{\sigma_o}{\pi} \left\{2 \tan^{-1} \frac{w}{s} - \frac{s}{w} \ln \left(1 + \frac{w^2}{s^2}\right)\right\} \qquad (2)$$

when $w >> s$ then $2 \tan^{-1} \frac{w}{s} \to \pi$ and $\frac{s}{w} \ln \left(1 + \frac{w^2}{s^2}\right) \to 0$. So, for a strip width that is much larger than the separation distance, the equation (2) reduces to equation (1).

Equation (2) is valid when the current is conducted in a sheet of zero thickness. Let us calculate the perpendicular force per unit area generated when the copper strips used are of finite thickness.

For the frequencies encountered in the current flow in the present experiments the current density in the copper strip is very nearly uniform across the conductor section. Thus the force produced is the result of integrating the forces due to conductor sheets across the thickness of the strip (for analysis see below).

If 2a is the thickness of copper strips and 2b is the width and if d is the separation distance between strips then the perpendicular force per unit area is given as

$$\sigma_2(\text{psi}) = \frac{2{\cdot}247 \times 10^{-8}\, i^2(\text{amp})}{b^2(\text{in})} \left[\frac{1}{8a^2} \left\{ (d + 2a)^2 - \frac{4b^2}{3} \right\} \tan^{-1} \frac{2b}{d + 2a} \right.$$

$$+ \frac{1}{8a^2} \left\{ (d - 2a)^2 - \frac{4b^2}{3} \right\} \tan^{-1} \frac{2b}{d - 2a} - \frac{1}{4a^2} \left(d^2 - \frac{4b^2}{3} \right) \tan^{-1} \frac{2b}{d}$$

$$- \frac{d}{16a^2 b} \left(4b^2 - \frac{d^2}{3} \right) \ln \left(\frac{d^2 + 4b^2}{d^2} \right) + \frac{(d + 2a)}{32a^2 b} \left\{ 4b^2 - \frac{(d + 2a)^2}{3} \right\}$$

$$\ln \left\{ \frac{(d + 2a)^2 + 4b^2}{d^2} \right\} + \frac{d - 2a}{32a^2 b} \left\{ 4b^2 - \frac{(d - 2a)^2}{3} \right\} \ln \left\{ \frac{(d - 2a^2) + 4b^2}{d^2} \right\}$$

$$\left. + \frac{(d + 2a)^3}{48a^2 b} \ln \left(\frac{d + 2a}{d} \right) + \frac{(d - 2a)^3}{48a^2 b} \ln \left(\frac{d - 2a}{d} \right) \right]$$

The results of the calculated perpendicular force per unit area for the three cases (eqs. 1, 2 and 3) are shown in figure 21 for a strip of width 0.25 in. This result shows that when the strip separation becomes large the perpendicular force per unit area drops significantly and the effect of finite thickness of copper strip is to reduce the perpendicular force per unit area.

The loading pulse obtained from the electromagnetic loading device is of 180 μsec duration. Using Fourier analysis we have obtained the frequency

components in this pulse. The major frequency values are 6250 Hz (58.5%), 18,750 Hz (33.1%) and 31,250 Hz (7.6%). Current in the copper strip is confined to surface only for high frequencies (skin depth). We have calculated the skin depth for the three major frequency components in our loading pulse. If σ is the electrical conductivity of material, and μ is the permeability then the skin depth δ for frequency f is given as

$$\delta = \left(\frac{2}{\mu\sigma\omega}\right)^{1/2}$$

for copper, $\sigma = 5.88 \times 10^{7}$

$\mu = 1.26 \times 10^{-6}$

$\omega = 2\pi f$

f (cycles/sec)	contribution (total 1.0)	skin depth δ (mm)
6,250	0.585	0.829
18,750	0.331	0.479
31,250	0.076	0.371

The copper strip used in our experiment was of 0.51 mm thickness. The skin depth calculations show that the current will flow essentially in the full thickness of the strip. So, the perpendicular force calucations are still valid even with the presence of high frequency components in the loading pulse.

We have taken some high speed photographs of the copper strip separating under dynamic load. Figure 22 shows this. It is obvious from this sequence of photographs that separation becomes large ($\simeq$ 0.5 in.) under dynamic load and that, therefore, Solithane cannot exploit all of the electromagnetic pressure. This explains why we were not able to easily propagate a crack

in Solithane under average loads (few thousand psi). Figure 23 shows the copper strip separation when circular polariscope was used. This photograph shows the fringe pattern for a given copper strip separation. The framing rate used was 50,000 frames/sec. Because of not getting a running crack in Solithane with our experimental set-up, we photographed the fringes near the crack tip under dynamic load with circular polariscope set-up (fig. 24). The fringes show the stress distribution ahead of the crack tip. The stress wave velocity in Solithane is relatively small and waves get highly attenuated. If the stress wave speed is, say, 10^4 in/sec and the pulse is for 180 μsec, then stress waves will travel 1.8 in. If we assume that the crack velocity is 0.33 of stress wave speed then the crack will move 0.6 in. At that point the unloading wave will catch up with the crack tip and will stop crack growth. Hence the observation of a running crack is not feasible with the current loading rate and the loading duration. By cooling the Solithane to about 0^oC will help to solve this problem. The modulus will become higher at such temperatures. This will enable us to observe running crack and crack branching.

A few times we were able to grow a crack by about 1 in. in length in Solithane which was observed with 100,000 frames per second, and the opening of the crack could be seen (fig. 25). We also examined the fracture surface under an optical microscope and noticed that the fracture surface was not smooth, but rather had some failures (fig. 26). We then took scanning electron microscope pictures of the fracture surface as shown in figs. 27-34. The fracture surface shown in figs. 27-31 was created under high rates of strain. By contrast the fracture shown in figs. 32-34 was created when the specimen was left at low load (but after application of dynamic load) for several days (time dependent). From the photographs of the fracture surfaces

it appears that the surface features are different for high speed fracture surface and the surface created slowly. Secondly there appears to be loose particles being created on the surface during the fracture process. The size of particles appears to be several microns. We have measured the step height of the fracture bands seen in the photograph. The maximum height appears to be about 20 μm.

REFERENCES

1. W. G. Knauss, "The Mechanics of Fracture," ed. by F. Erdogan, AMD-Vol. 19, Amer. Soc. of Mech. Engineers, NY, 1976.

2. W. G. Knauss, "Deformation and Fracture of High Polymers," ed. by H. Henning Kausch, John A. Hassell and Robert I. Jaffee. Plenum Press, 1974.

3. W. G. Knauss and H. K. Mueller, "The Mechanical Characterization of Solithane 113 in the Swollen and Unswollen State," GALCIT SM 67-8, California Institute of Technology, AFRPL-TR-68-125.

4. James W. Dally and William F. Riley, "Experimental Stress Analysis," 2nd ed., McGraw Hill Book Col, 1978, p. 406.

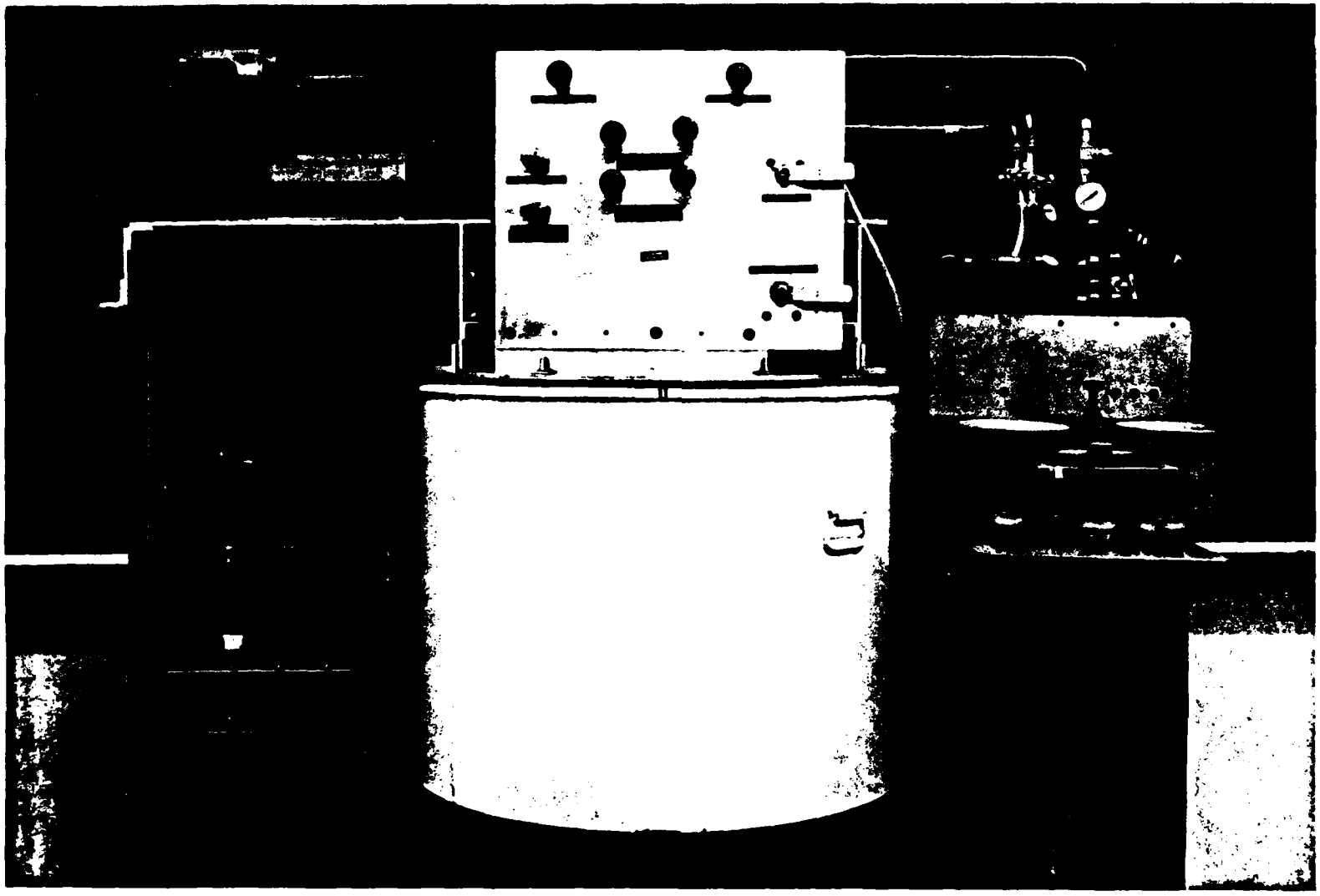

Fig. 1. Solithane Casting Facility

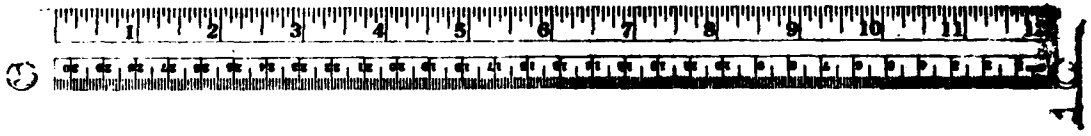

Fig. 2. Solithane Plate 12 x 12 x 0.25 (inch)

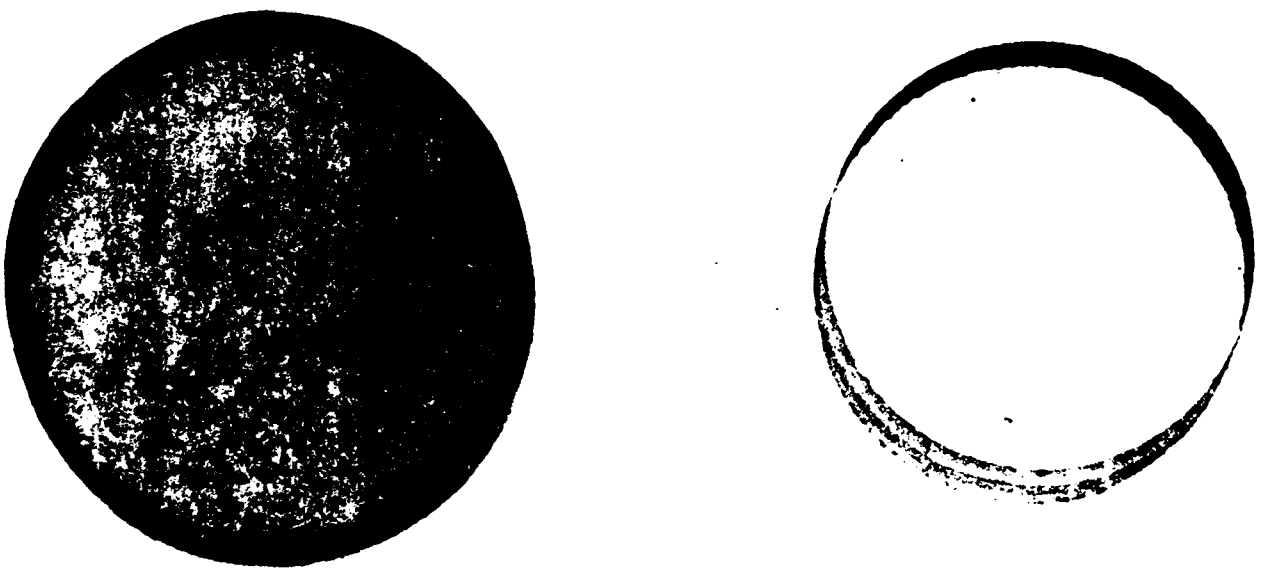

Fig. 3. (a) Glass Bead Filled Solithane (b) No Glass Bead in Solithane

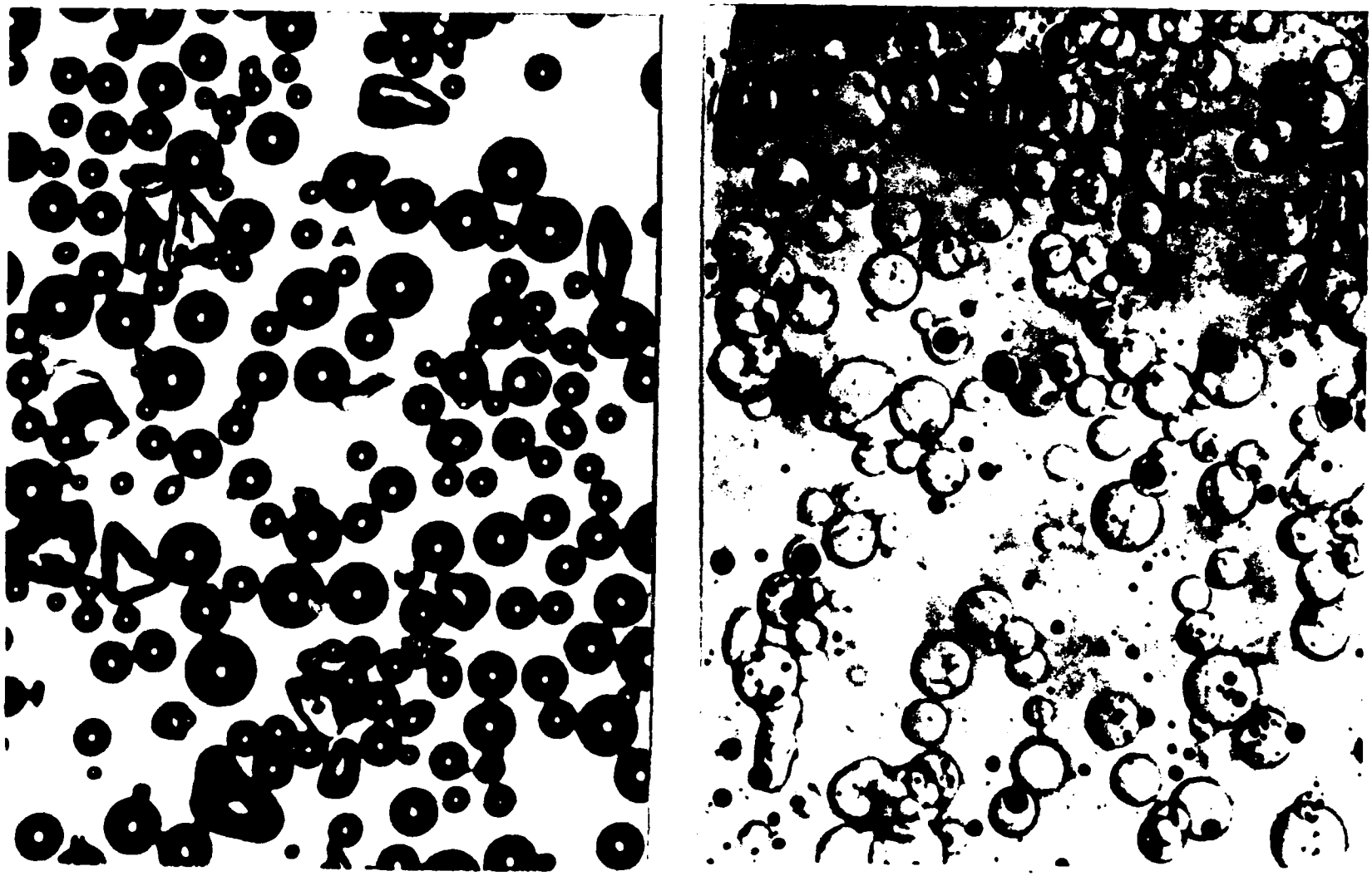

Fig. 4. (a) Glass Beads Photographed in Air (b) Glass Beads in Solithane

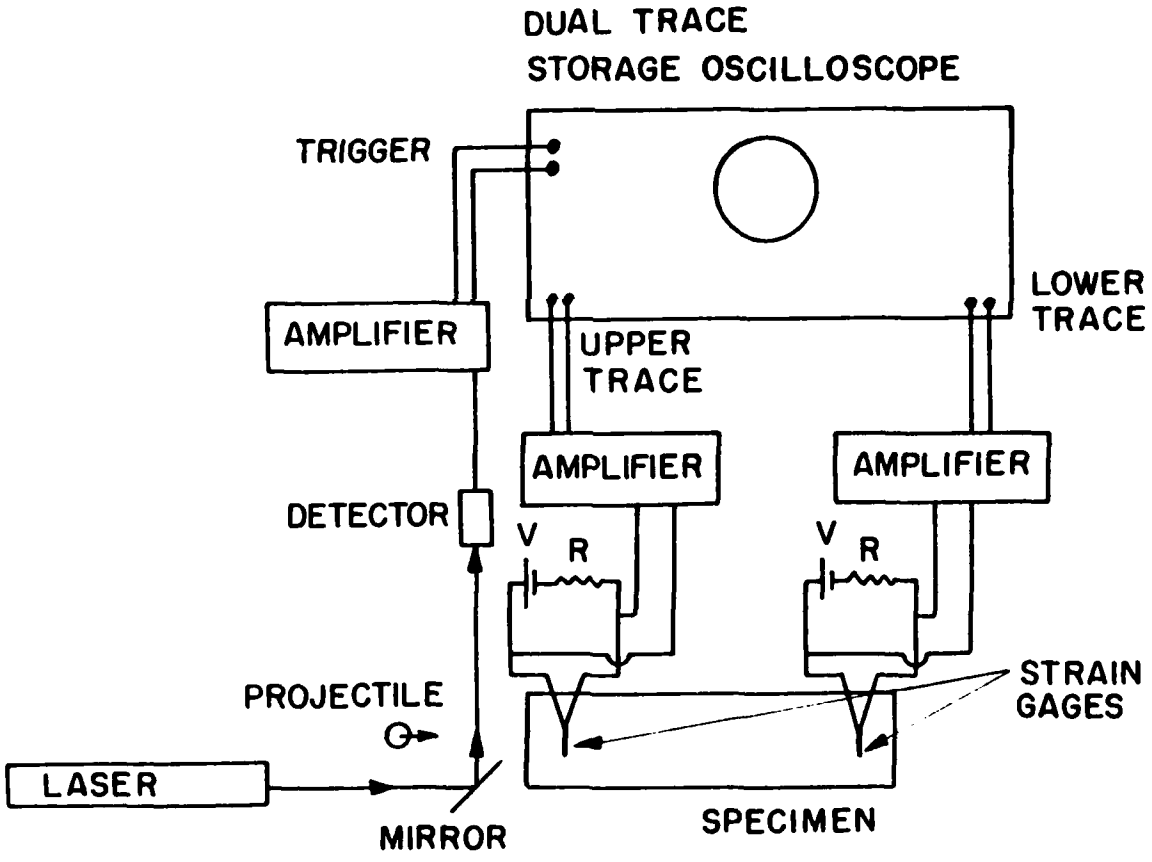

Fig. 5. Experimental Set Up for Stress Wave Passage through Each Strain Gage

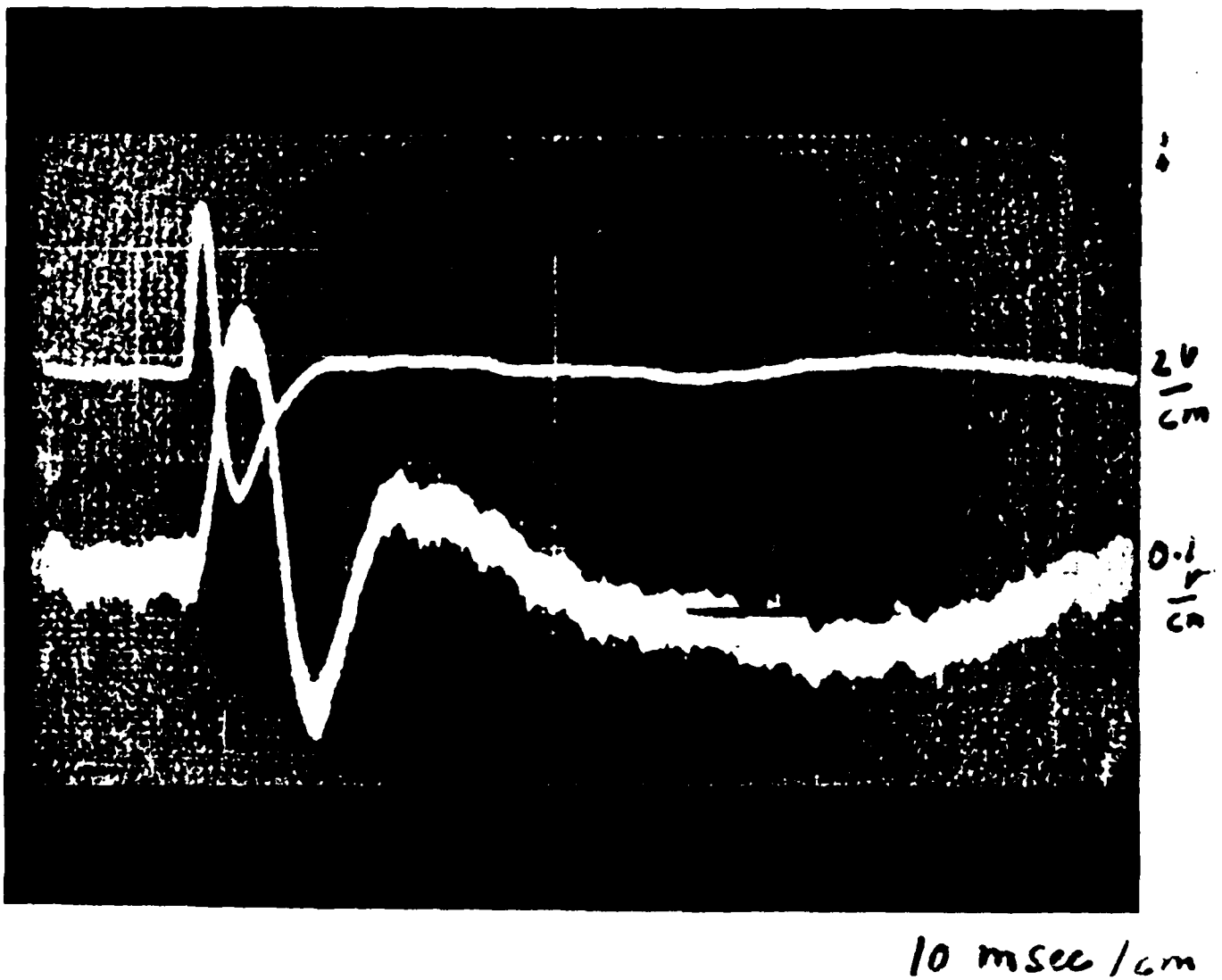

Fig. 6. Strain Gage Output Showing the Stress Wave Passage through Each Strain Gage

P Polarizer

QP Quarter Plate

A Analyzer

S Specimen

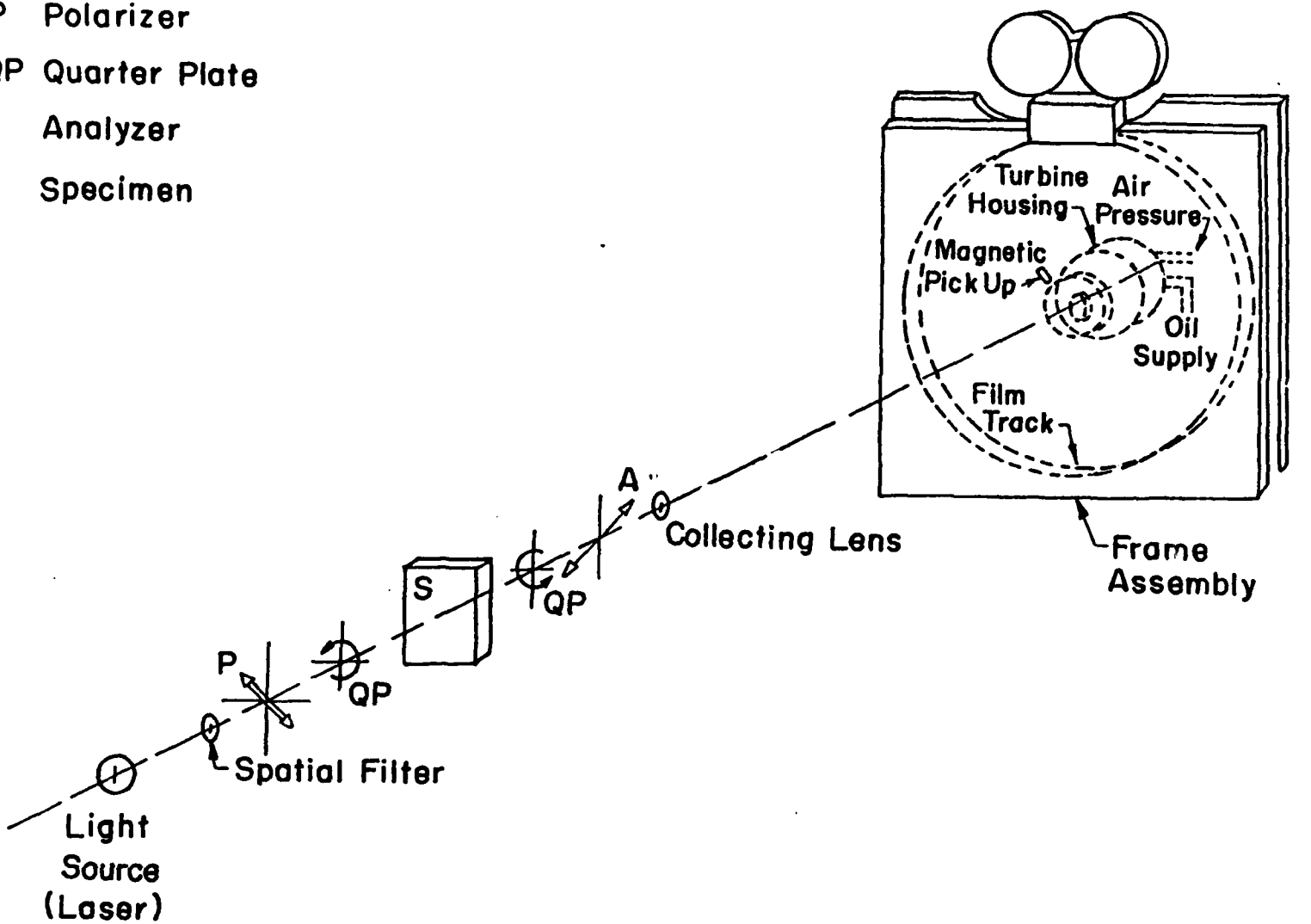

FIG. 7 EXPERIMENTAL SET UP FOR MEASUREMENT OF STRESS WAVE PROPAGATION USING PHOTOELASTIC EFFECT

Fig. 8. Experimental Set Up for Applying Loading Pulse

Fig. 9. Photoelastic Fringes in Solithane Obtained Under Dynamic Load. Time Interval Between (a) and (b) is 100 μ sec and Between (b) and (c) is 120 μ sec (Framing Rate 50,000 per second).

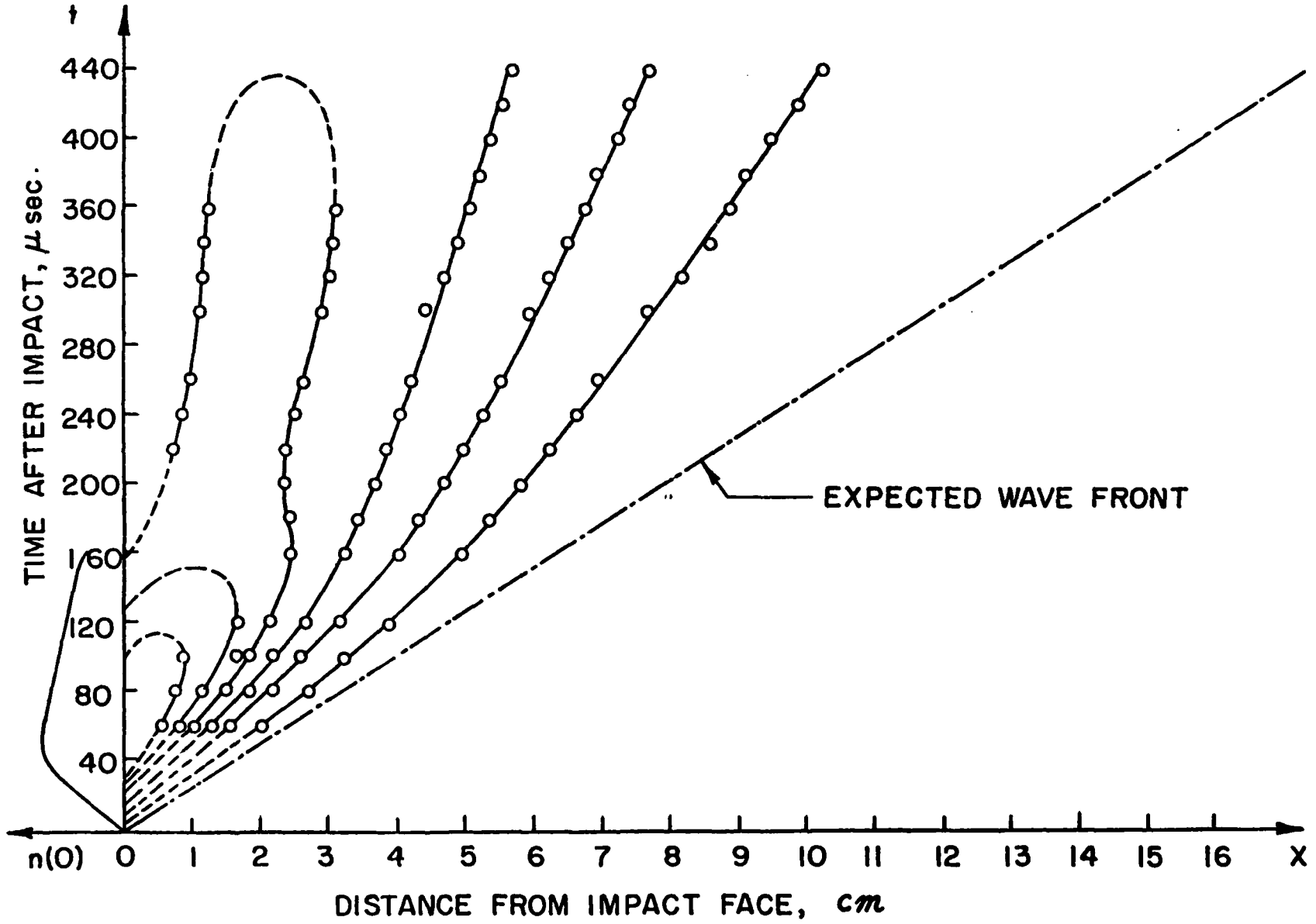

FIG.10. CONSTANT FRINGE CONTOUR FOR STRESS WAVE PROPAGATION IN A SOLITHANE PLATE

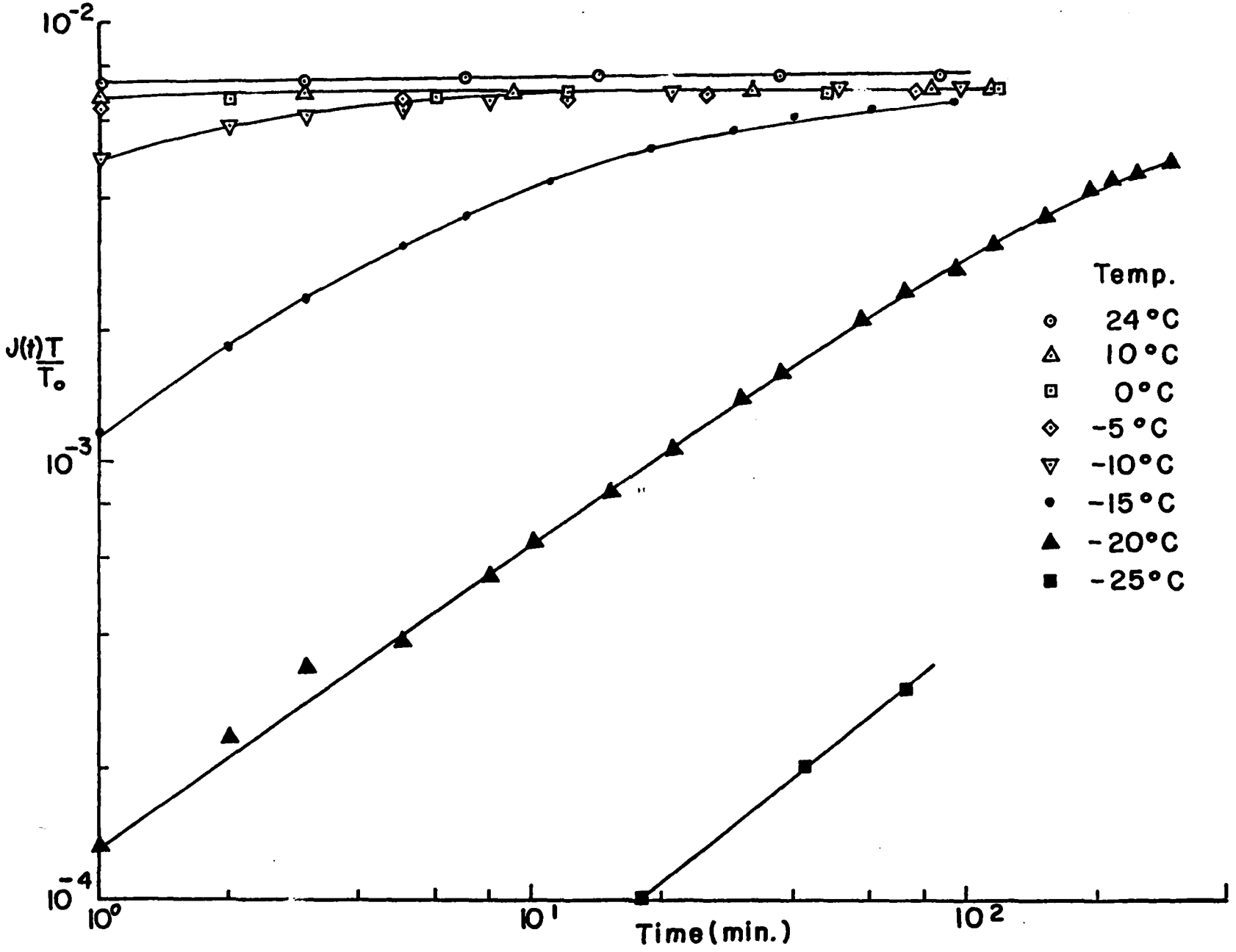

FIG. 11 SHEAR CREEP MEASUREMENTS ON SOLITHANE AT DIFFERENT TEMPERATURES (J IS SHEAR CREEP COMPLIANCE)

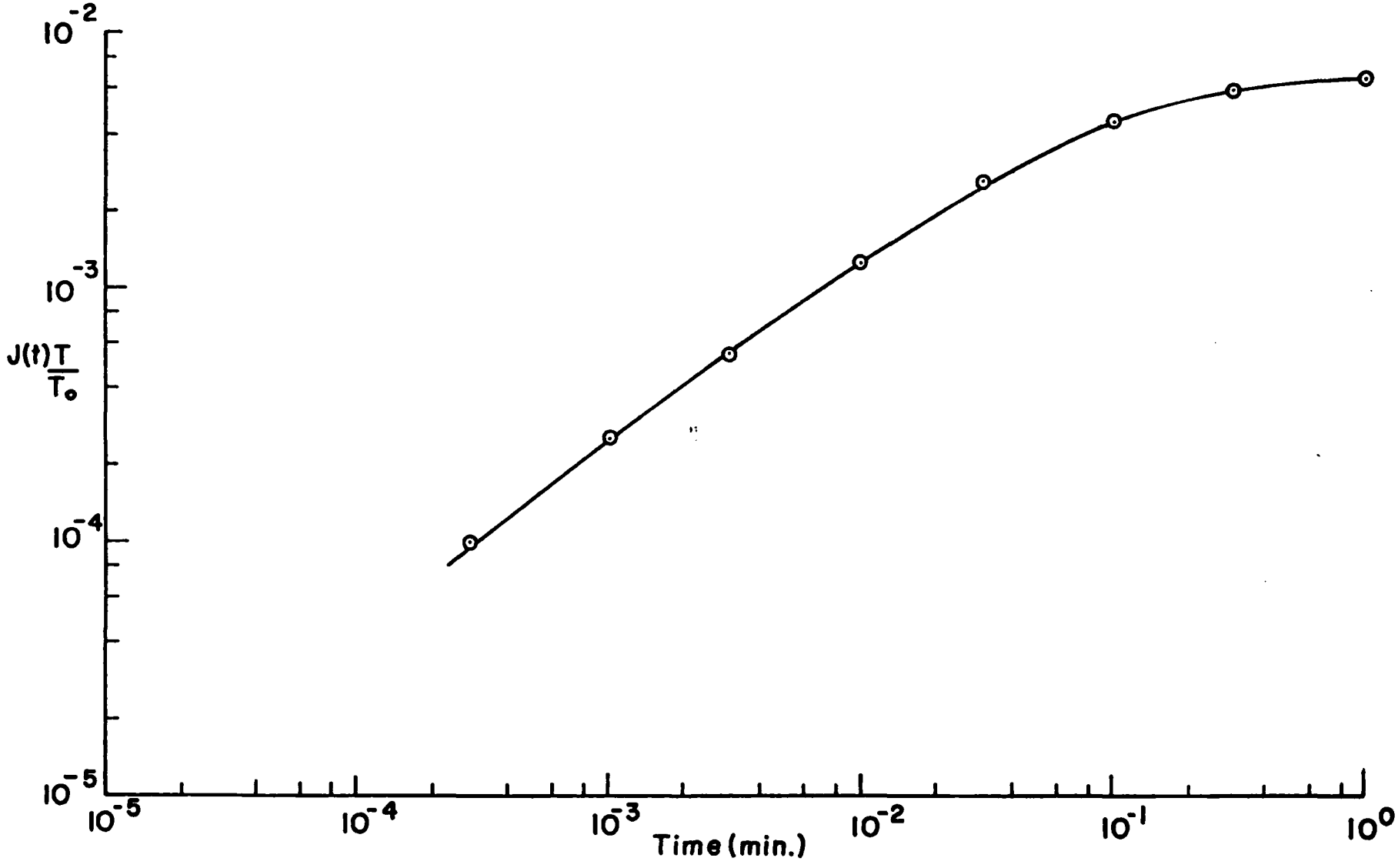

FIG. 12 MASTER CREEP CURVE FOR SOLITHANE OBTAINED USING TIME-TEMPERATURE SUPERPOSITION

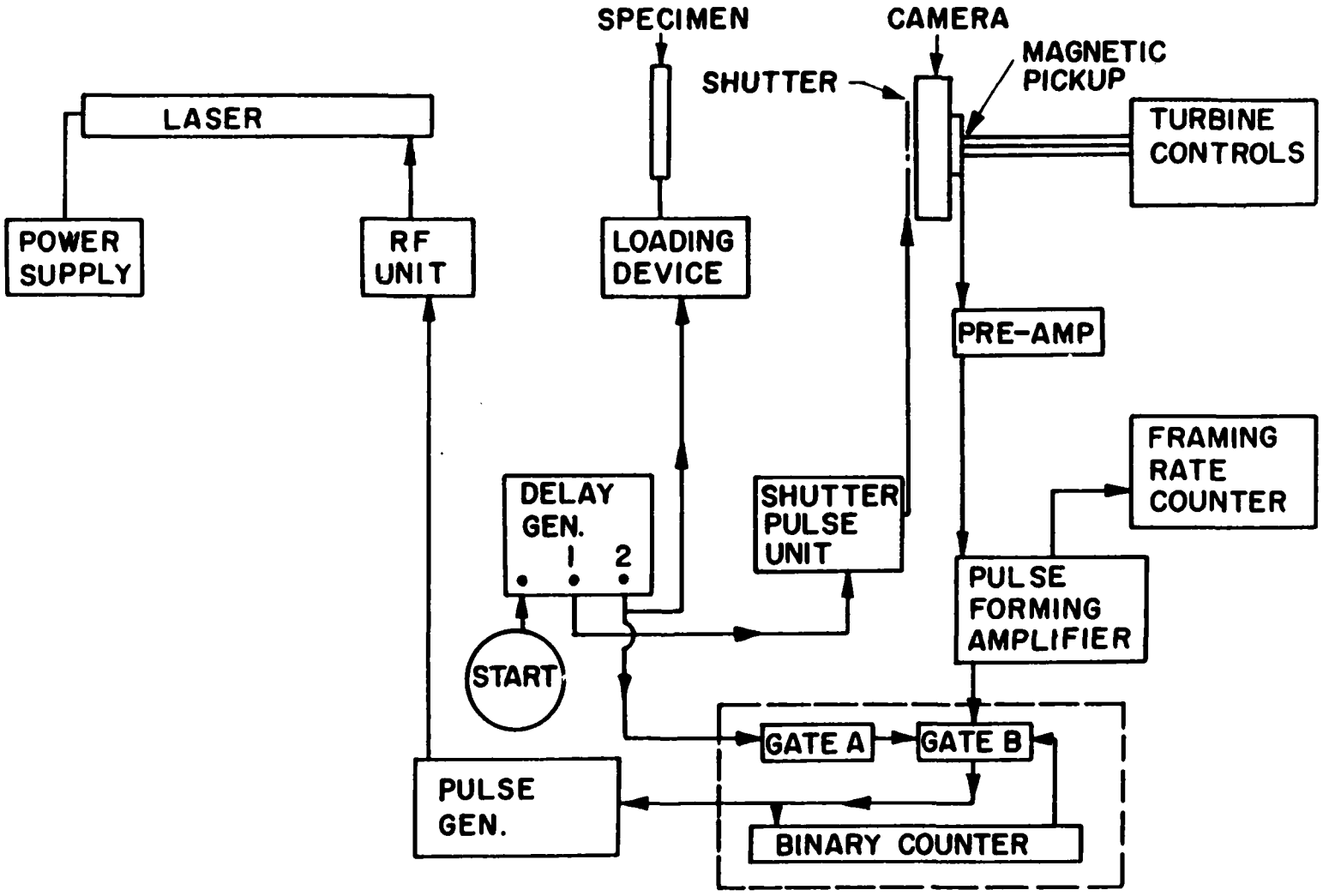

Fig. 13. Schematic Showing the Time Coordination of Laser with Electromagnetic Loading Device and High Speed Camera

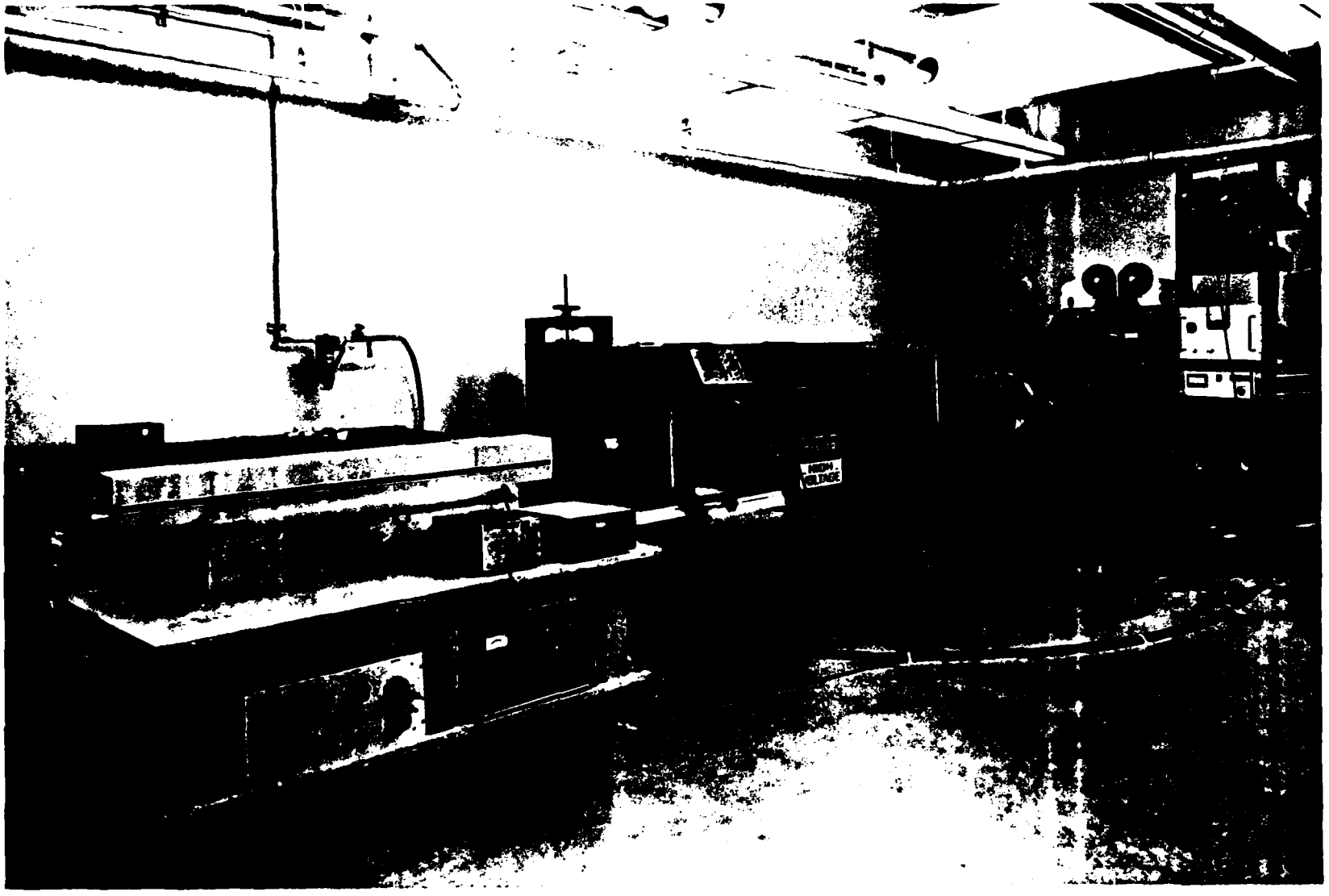

Fig. 14. Experimental Set Up for Dynamic Fracture Study

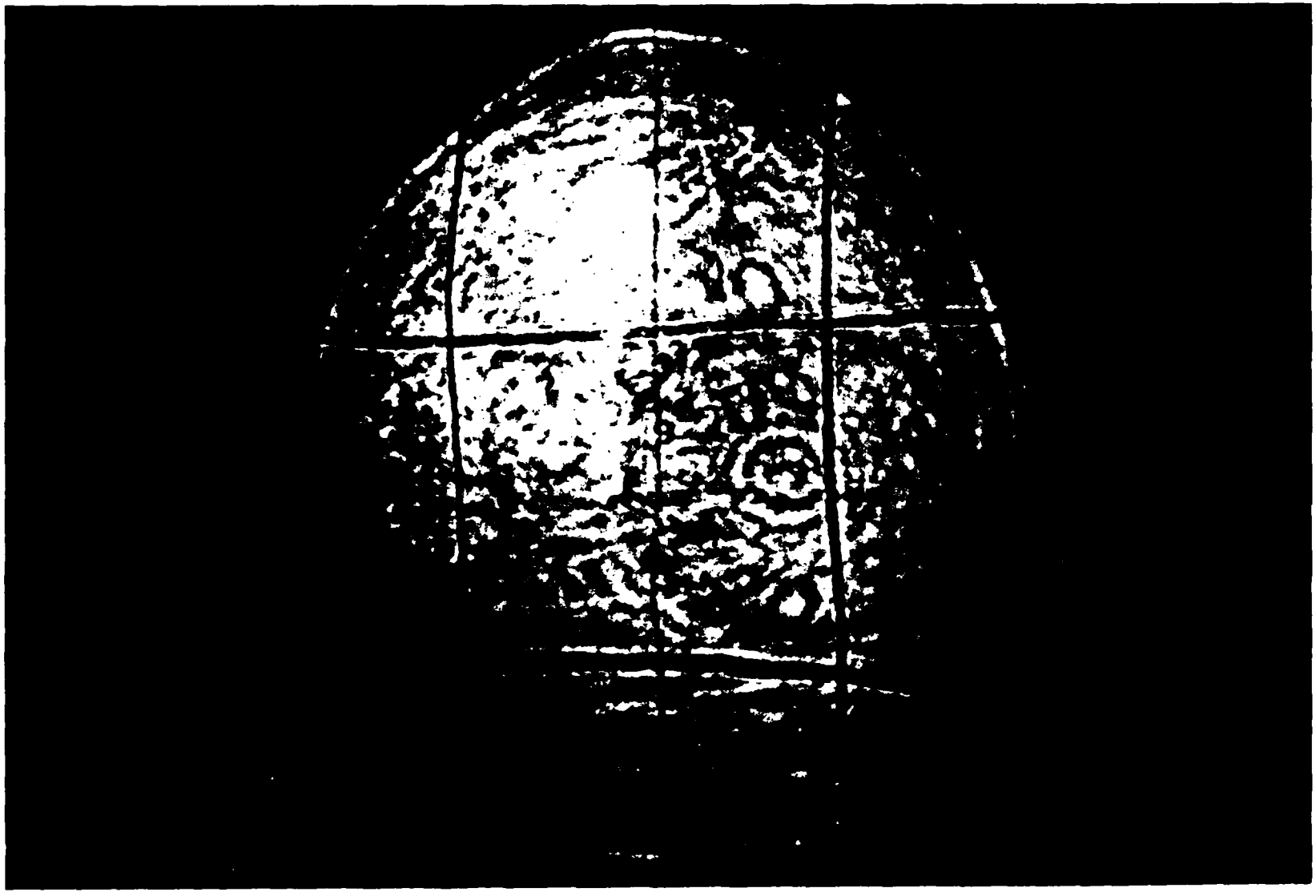

Fig. 15. High Speed Photograph of a Wire Grid Taken at a Framing Rate of 100,000 Frames/sec. Smallest Wire Photographed is Three Thousandth of an Inch.

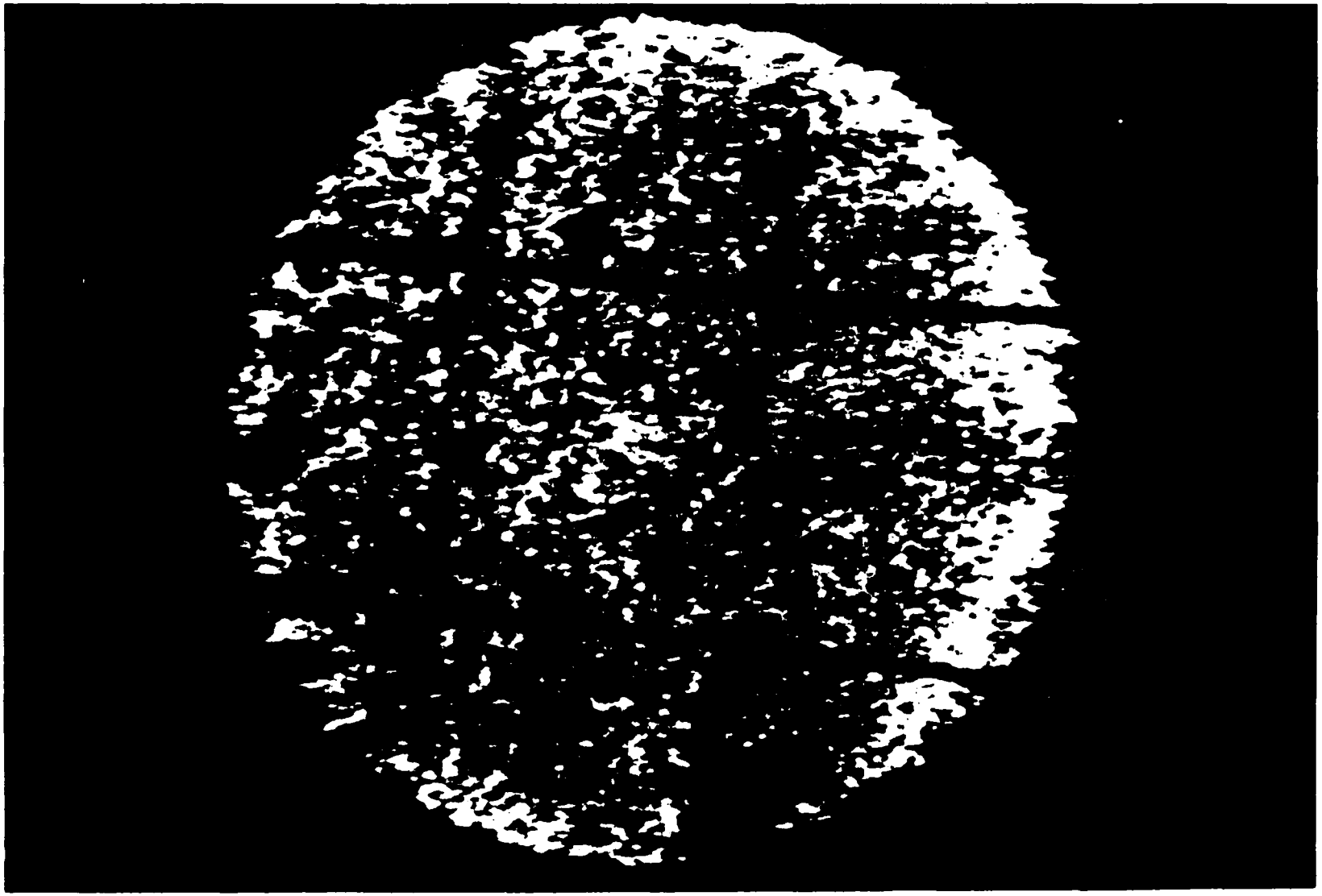

Fig. 16. High Speed Photograph of a Wire Grid Taken in Reflected Light

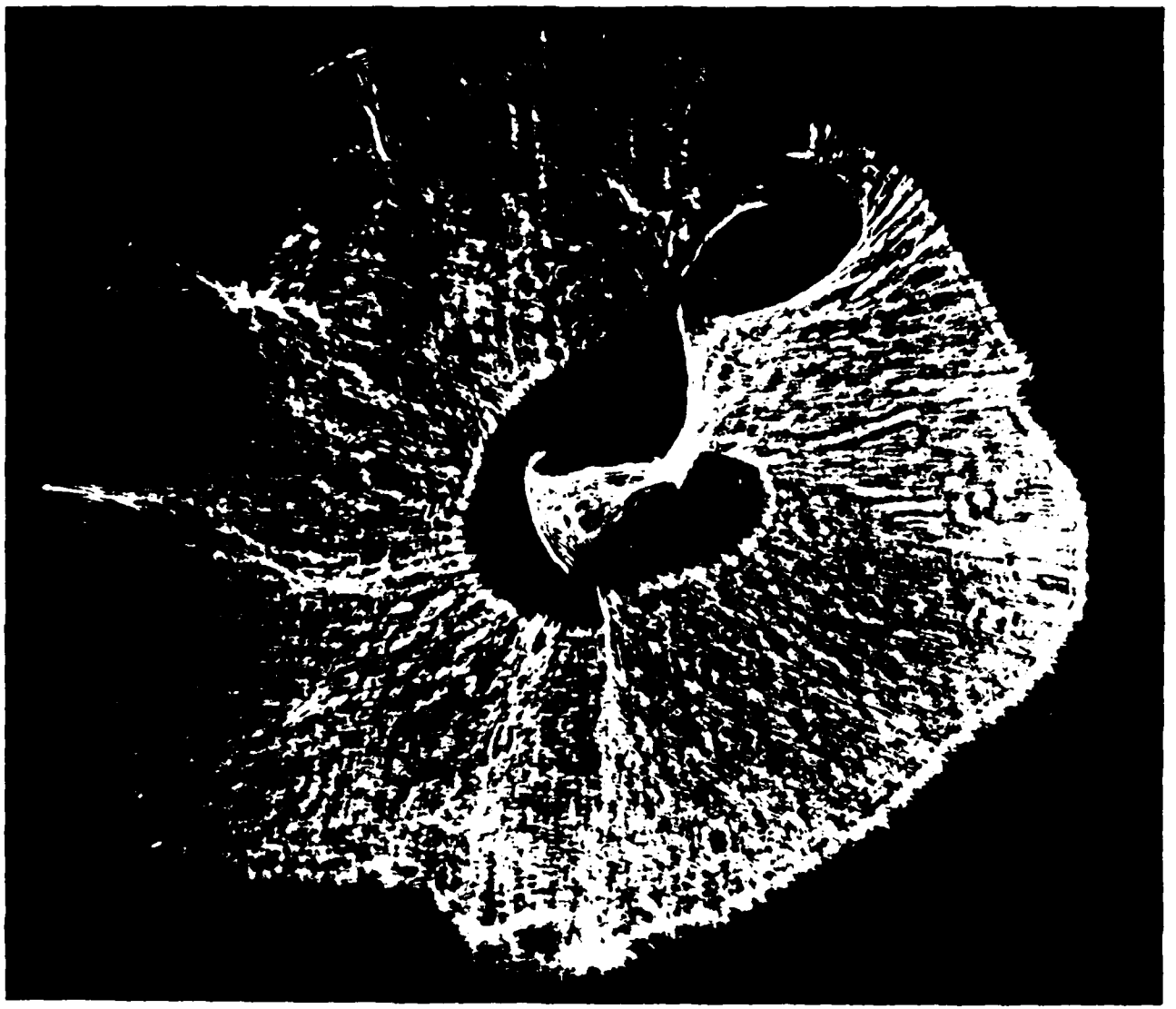

Fig. 17. Photograph of a Region Ahead of a Crack Tip with Curious Optical Structure

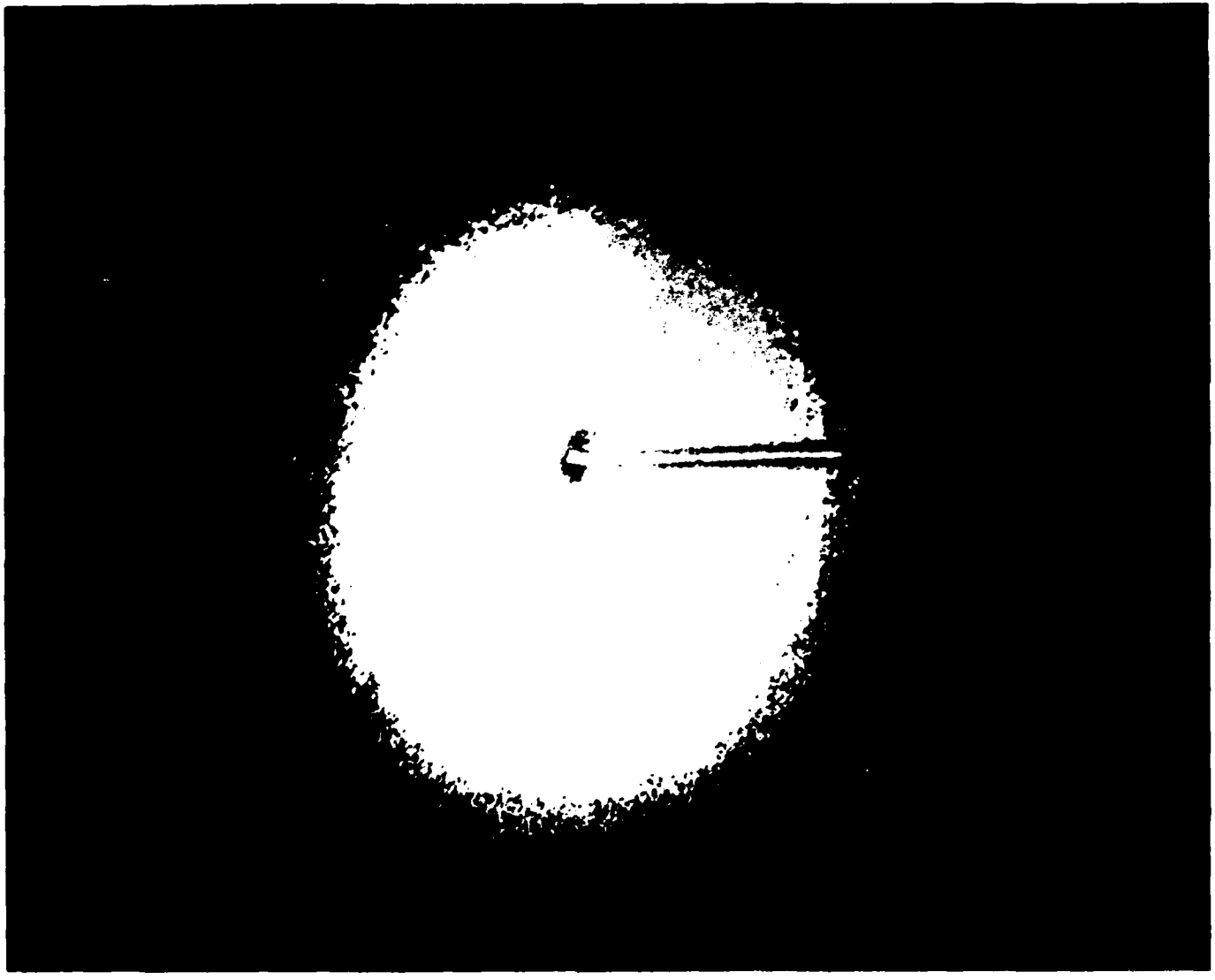

Fig. 18. Static Photograph of a Crack Tip in Solithane

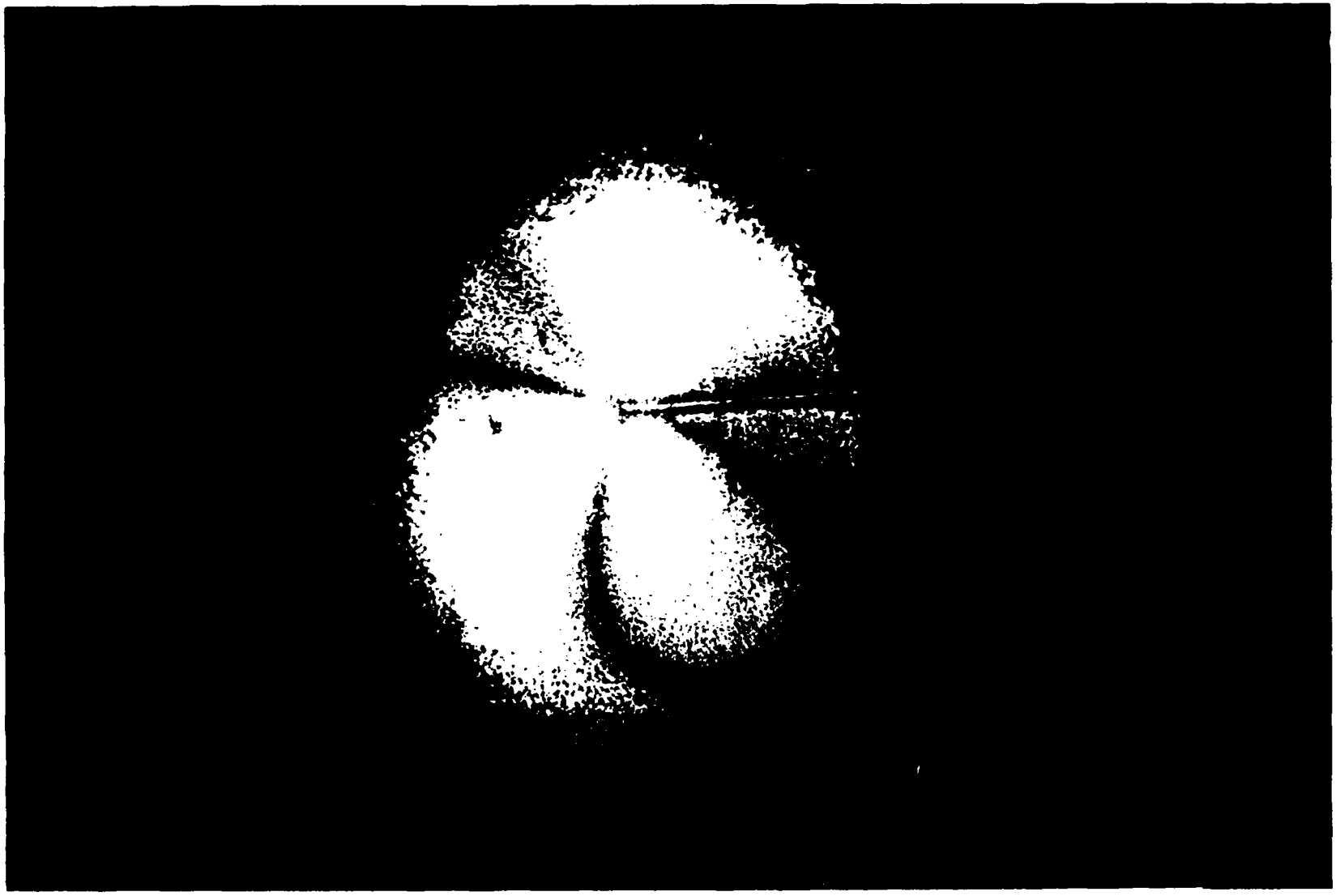

Fig. 19. Static Photograph of Crack Tip, Showing the Photoelastic Fringes

Fig. 20. Crack Propagation in Plexiglass Under Dynamic Load

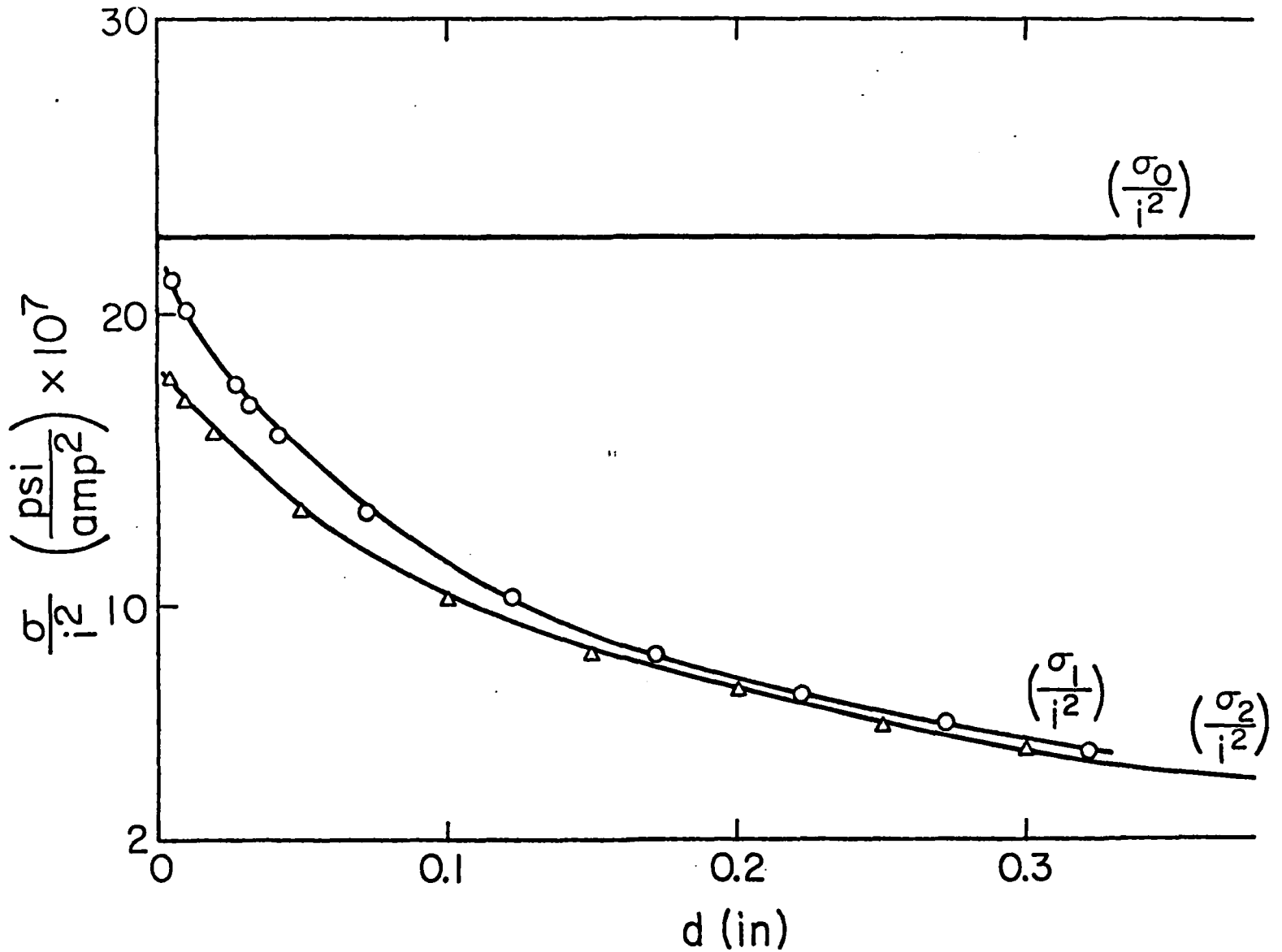

FIG. 21. Variation of σ_1, σ_2, and σ_3 with Copper Strip Separation Distance

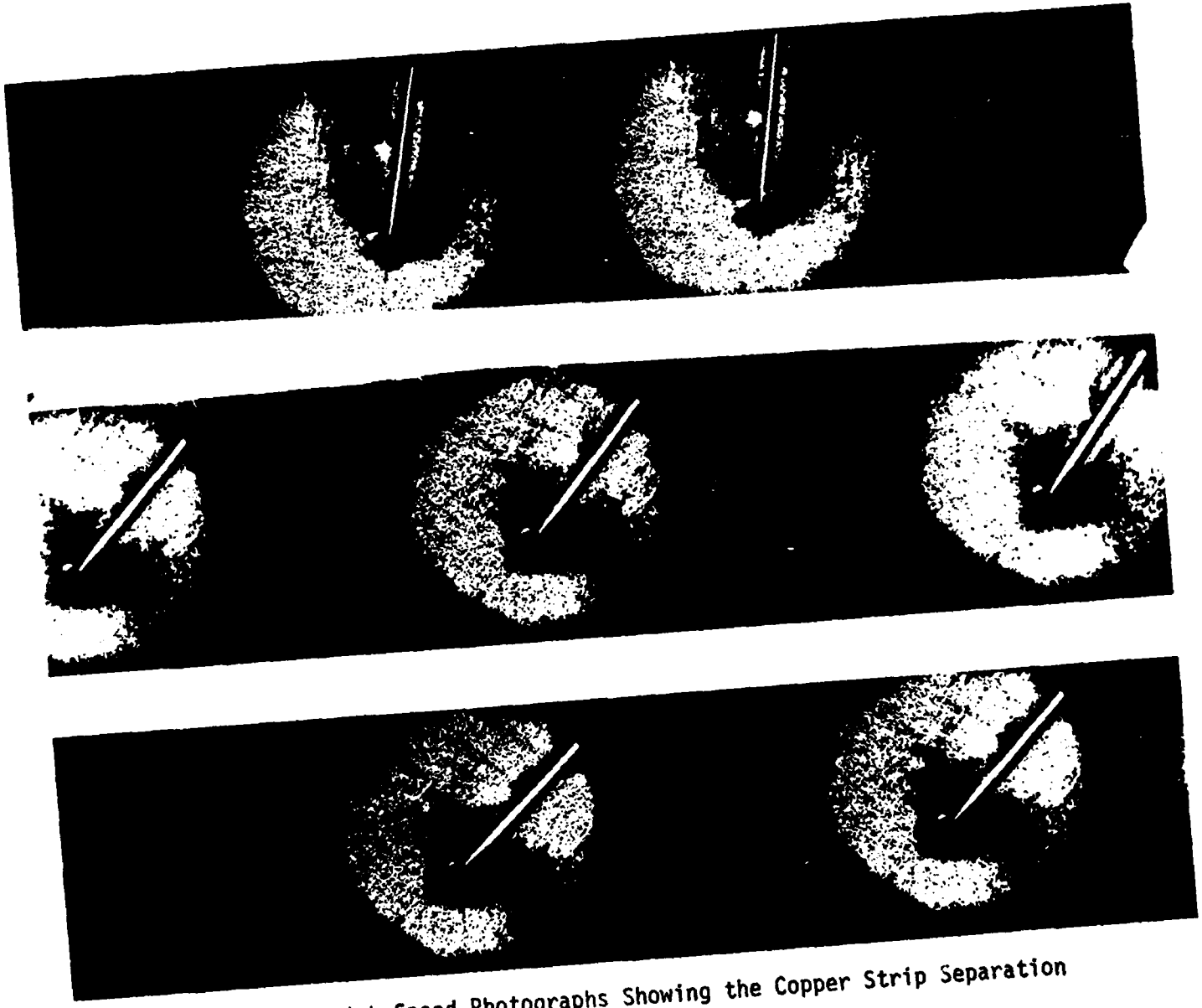

Fig. 22. High Speed Photographs Showing the Copper Strip Separation

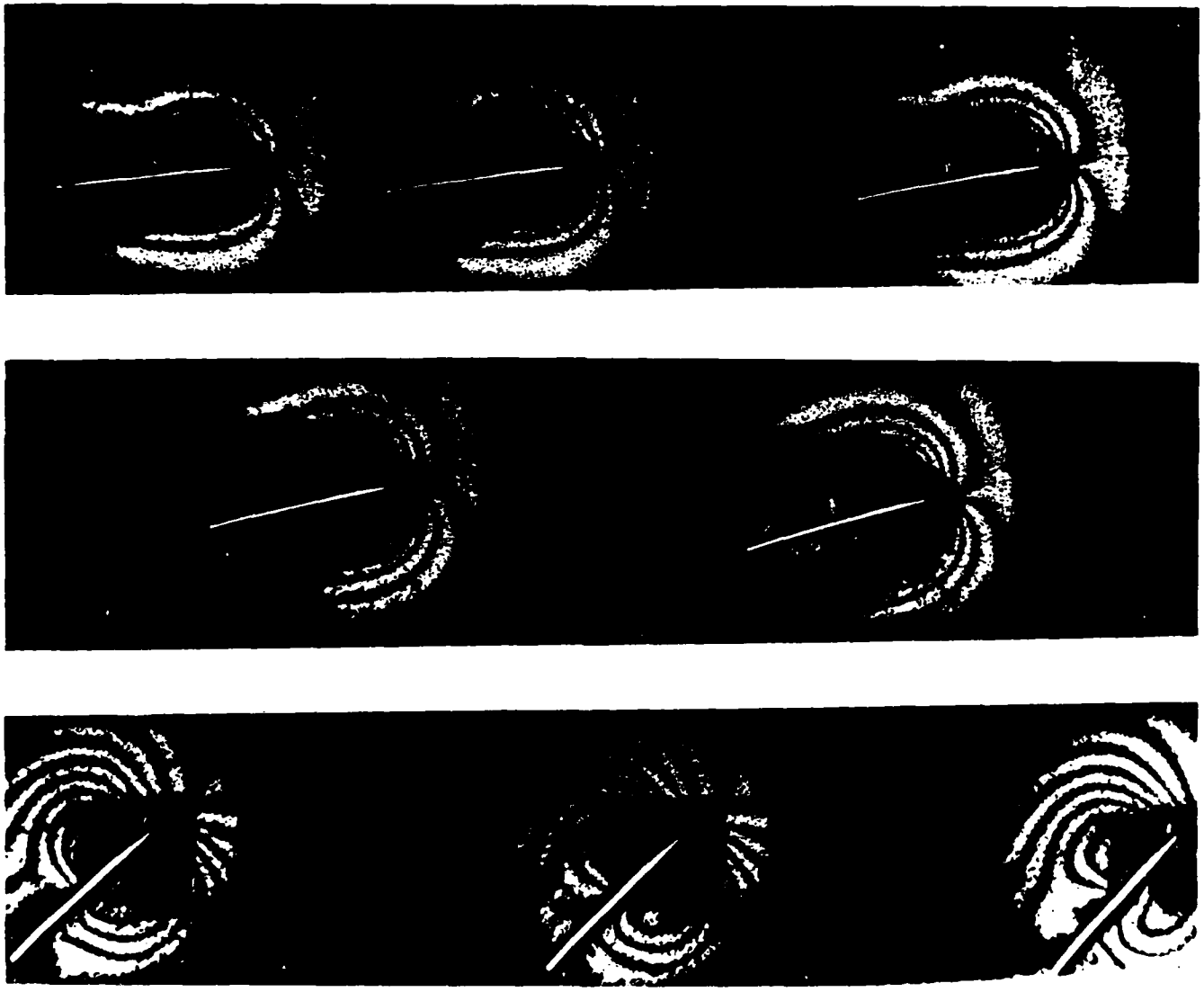

Fig. 23. High Speed Photograph of Copper Strip Separation with Photoelastic Fringes

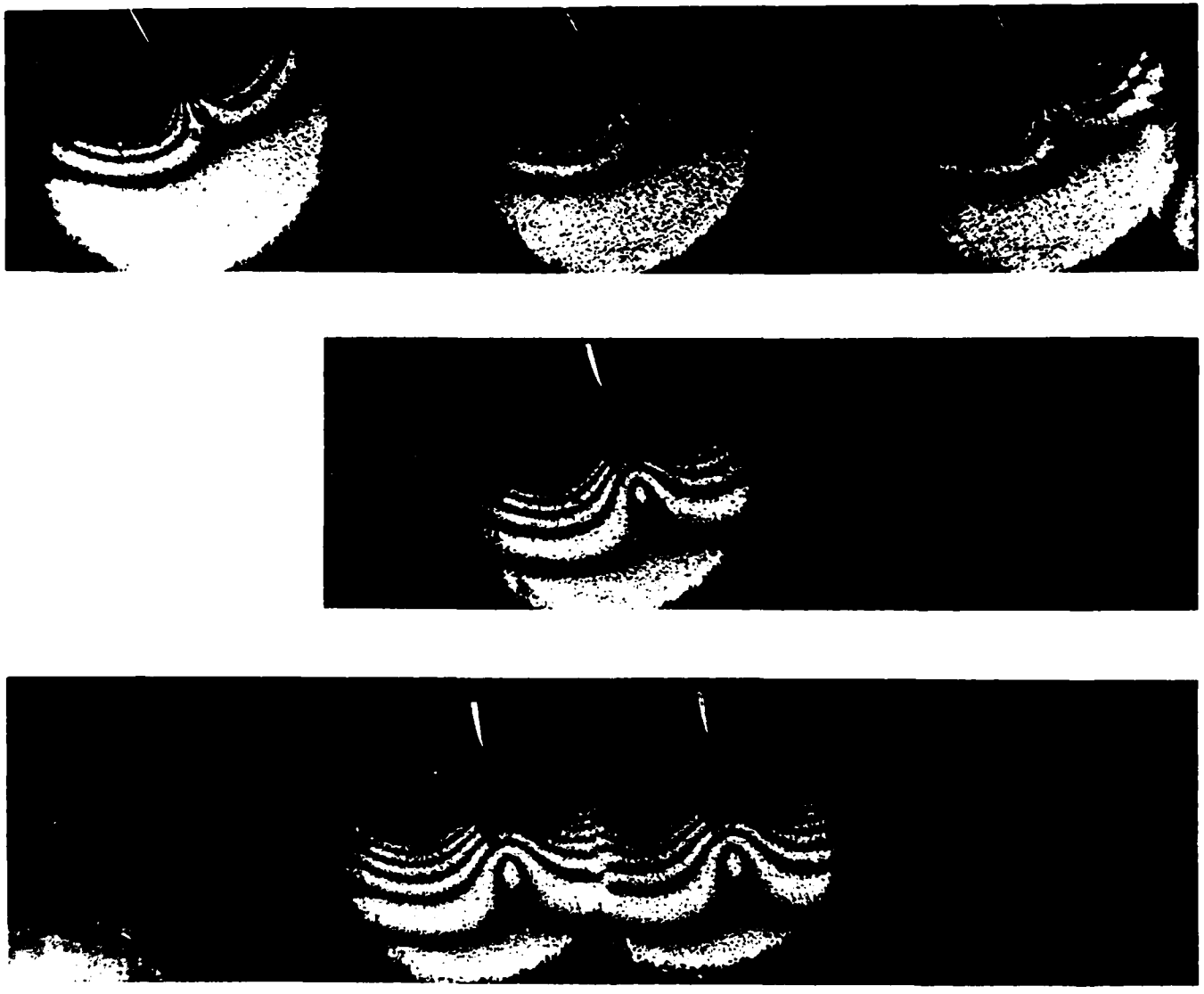

Fig. 24. High Speed Photograph of Photoelastic Fringes, ahead of a Crack Tip in Solithane

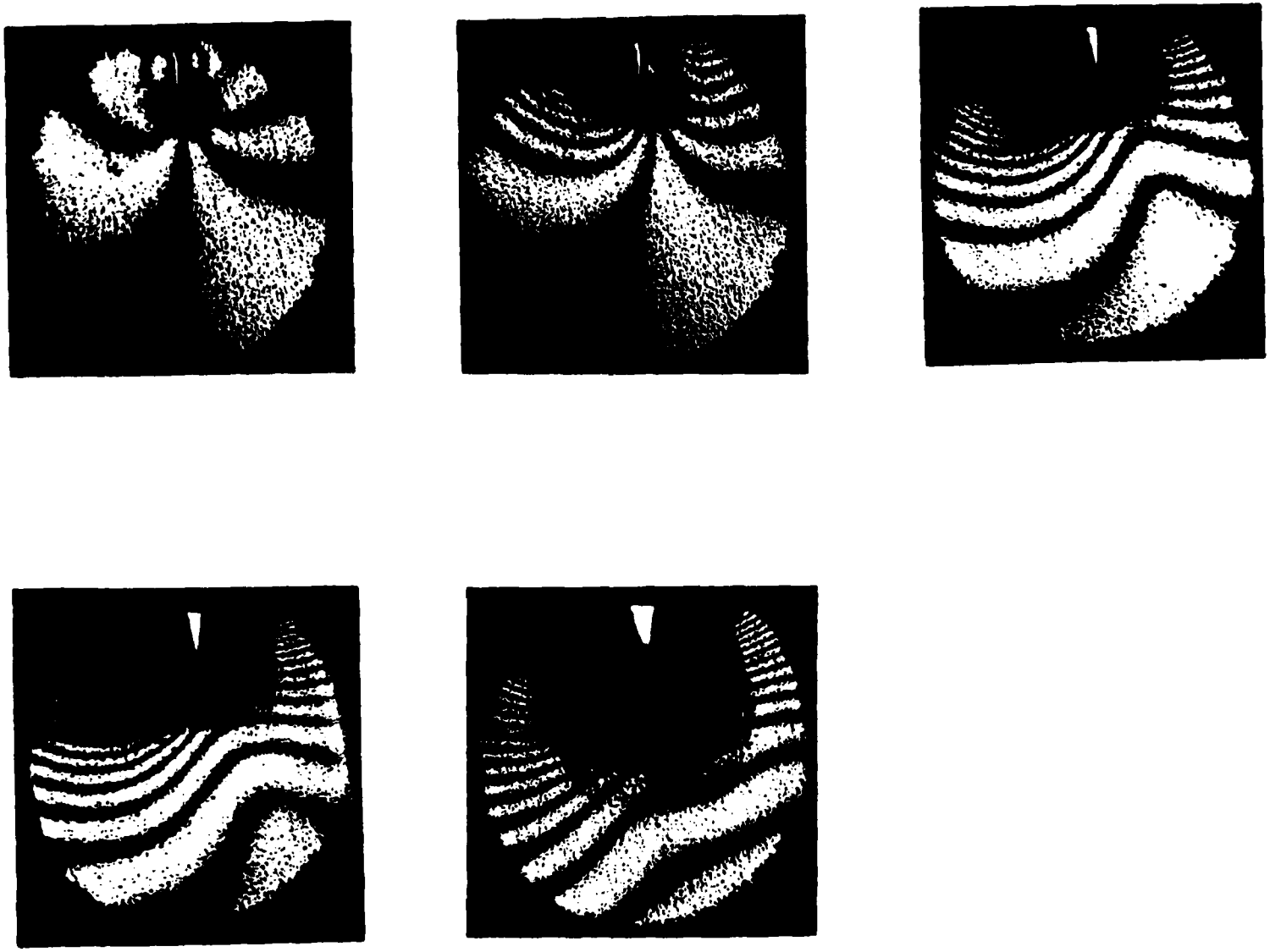

Fig. 25. Crack Opening Angle Under Dynamic Load

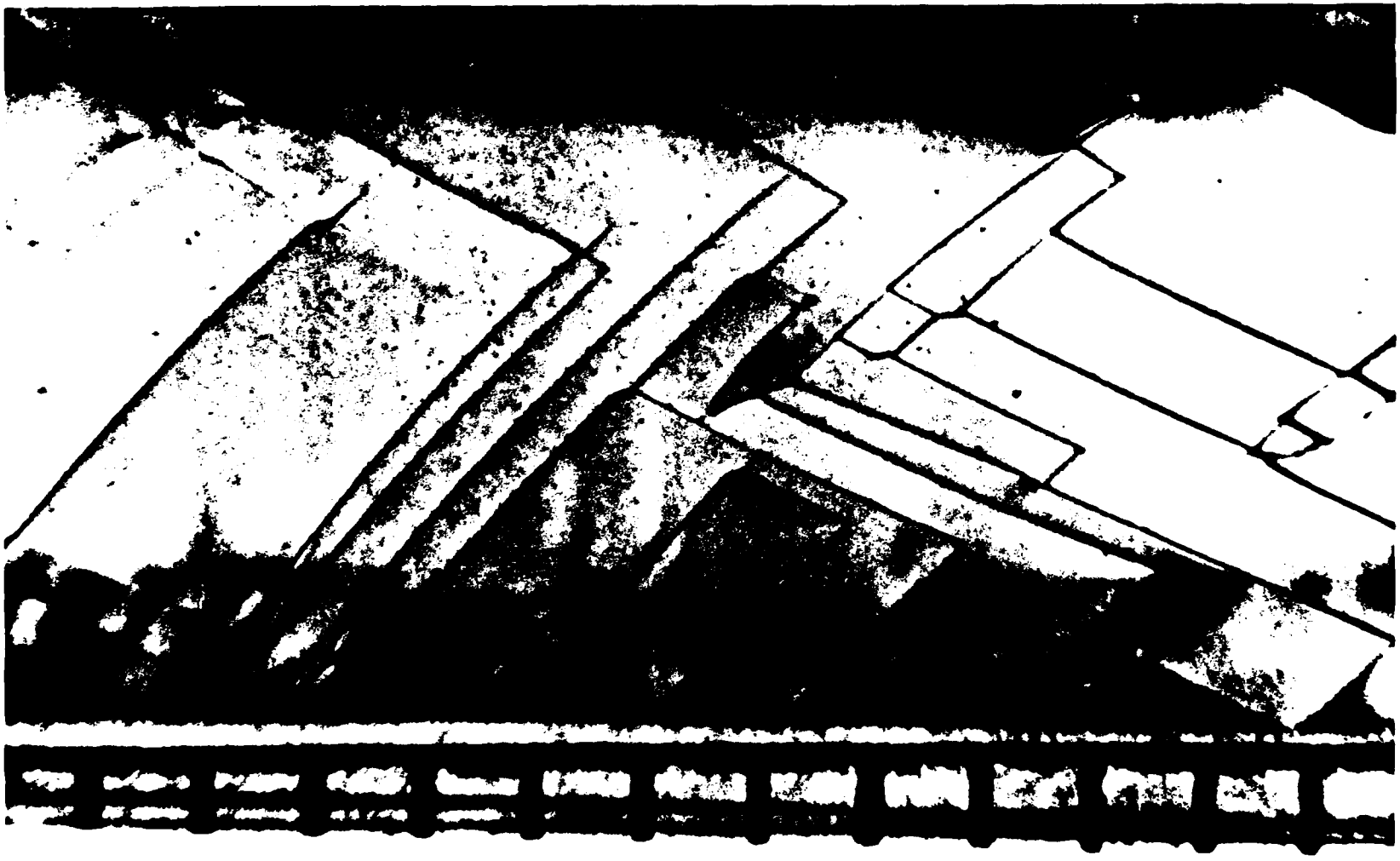

Fig. 26. Optical Microscope Picture of Fracture Surface

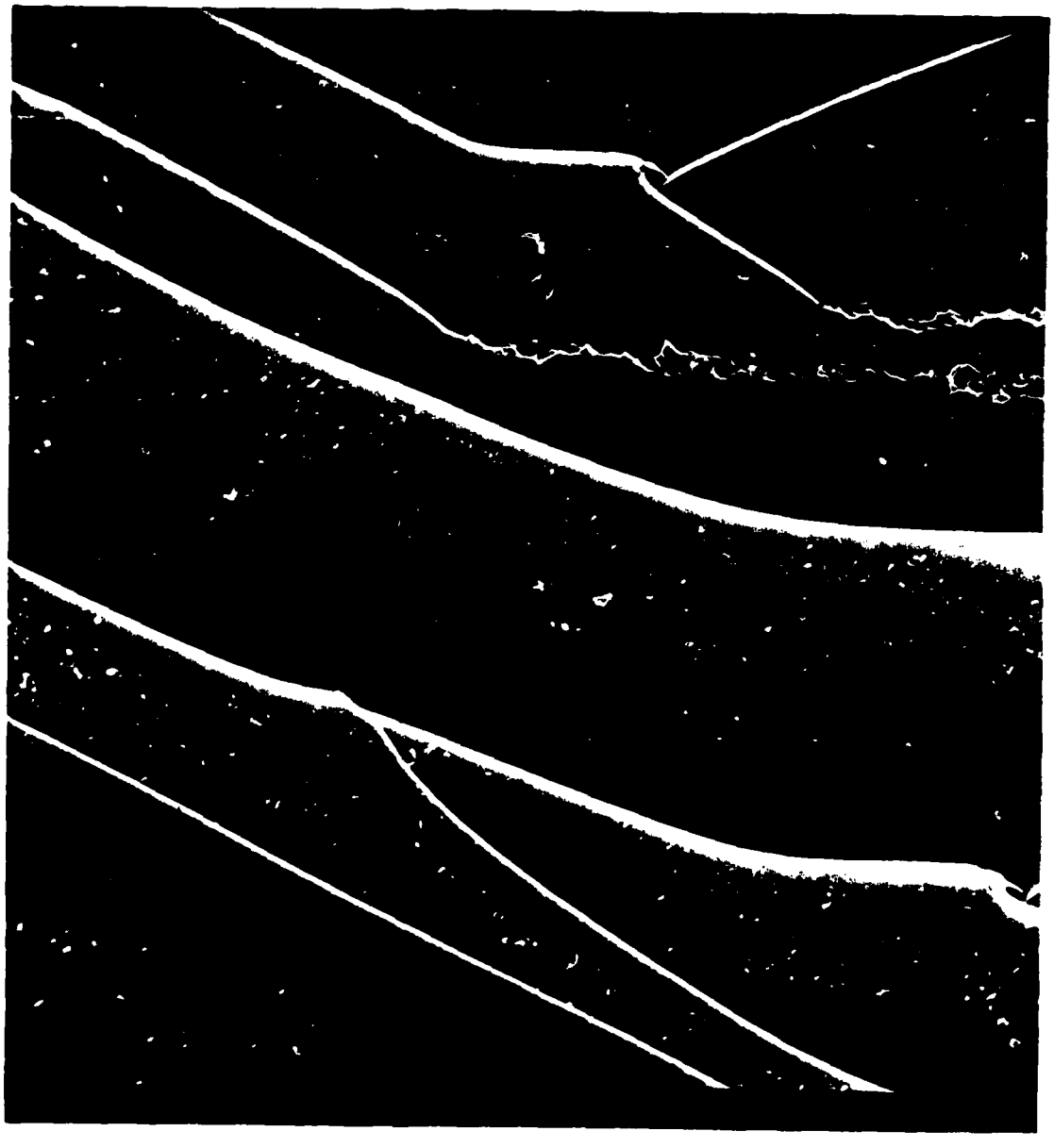

Fig. 27. Fracture Surface Created Due to Dynamic Load.
Crack Running from Right to Left (Magnification X20)

Fig. 28. High Speed Fracture Created Under Dynamic Load (Magnification 300X)

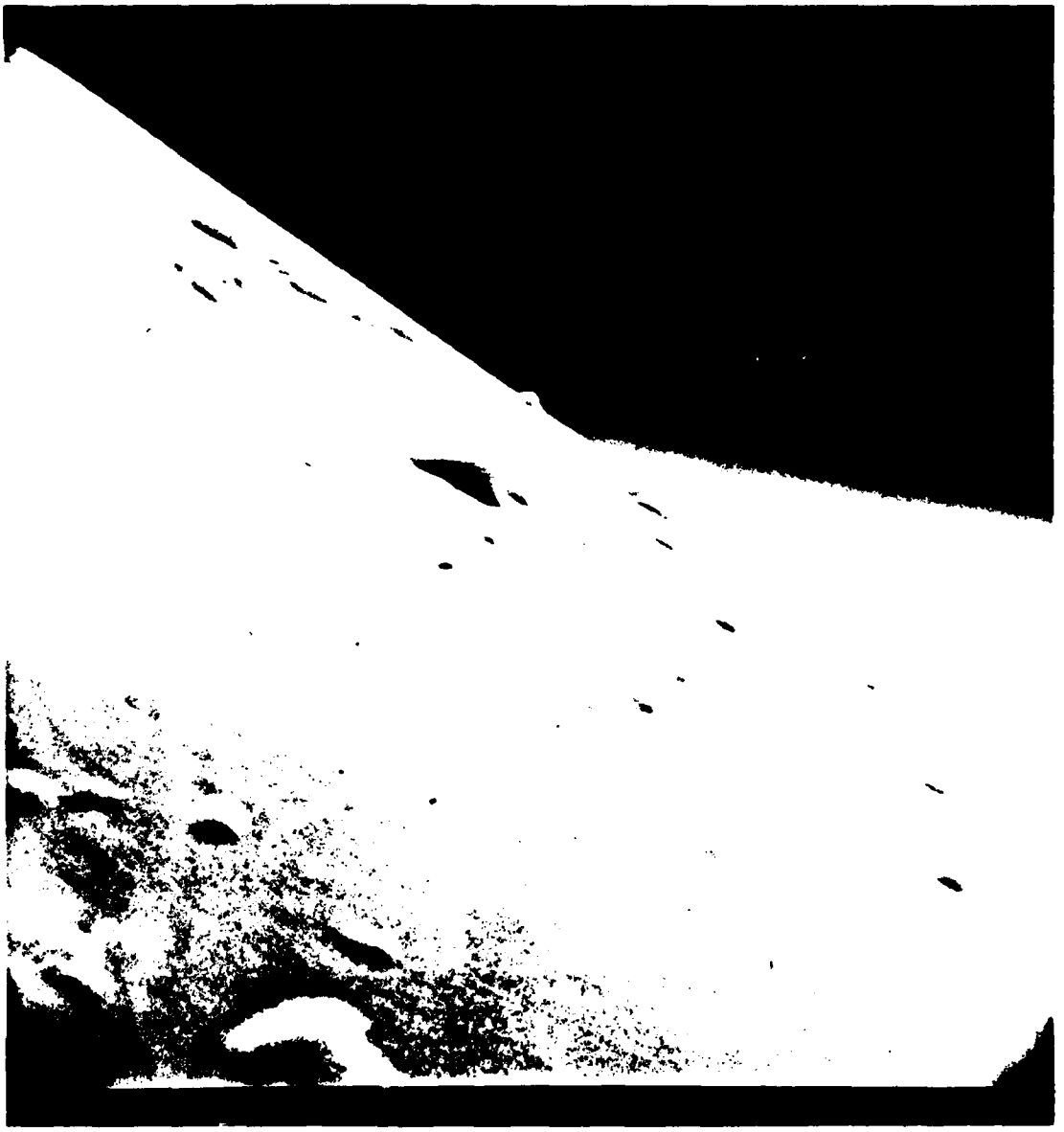

Fig. 29. Fracture Surface Created Due to Dynamic Load (Magnification 800X)

Fig. 30. Fracture Surface Created Under Dynamic Load (Magnification 2100X)

Fig. 31. Fracture Surface Created Due to Dynamic Load, Size of Particles on Fracture Surface is Shown Here. (Magnification 21,000)

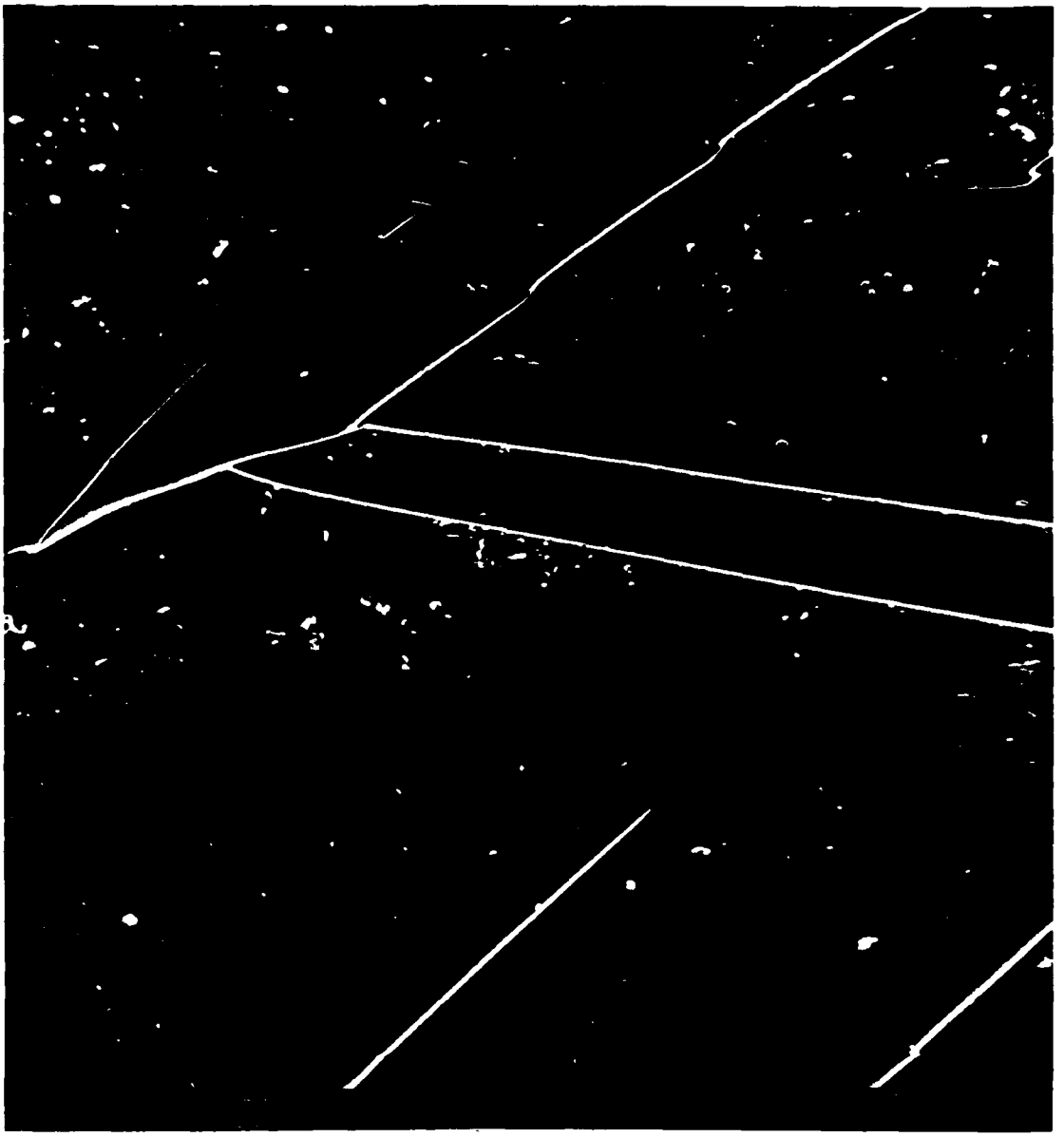

Fig. 32. Fracture Surface Created by Slow Growth. Crack is Moving from Right to Left (Magnification 30X).

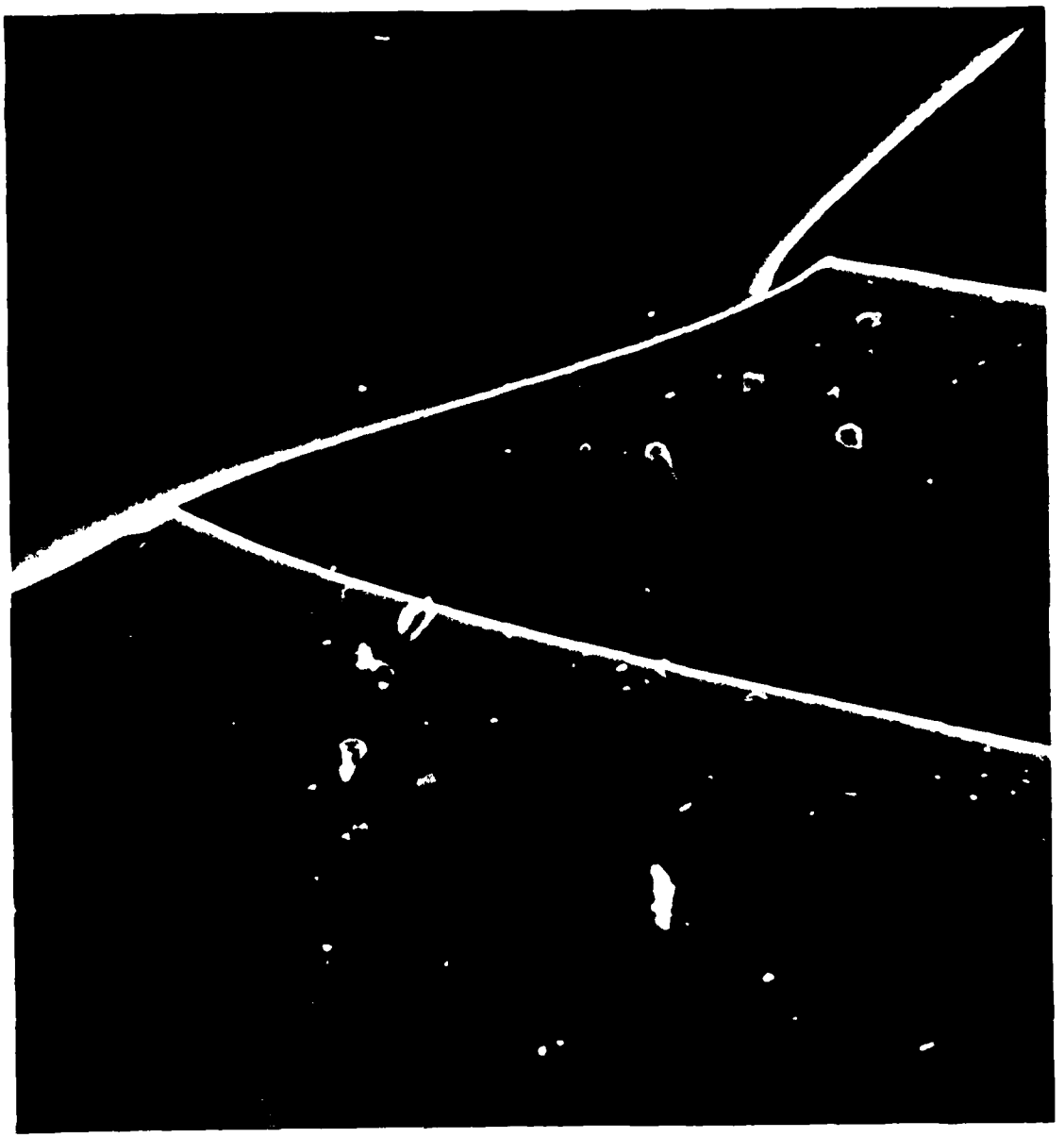

Fig. 33. Slow-Growth Fracture Surface (Magnification 180X)

Fig. 34. Time Dependent Fracture Surface (Magnification 1400)